Developmental candidate GHP-88310/EIDD-3608 with high tolerability and oral efficacy in measles and respiratory paramyxovirus models

Carolin M Lieber[1], Josef D Wolf[1], Mugunthan Govindarajan[2], Jeong-Joong Yoon[1], Zachary M Sticher[2], Claire E Ruckel[1], Alexander I Leach[1], Lauren A Harrison[1], Dariia Vyshenska[3], Amalia Anne Cruz[2], Meghan K. Andrews[2], Rebecca E. Krueger[2], Robert M Cox[1], George R Painter[2], Alexander L Greninger[3], Michael G Natchus[2], Richard K Plemper[1]*

[1]Center for Translational Antiviral Research, Georgia State University Institute for Biomedical Sciences, Atlanta, GA, 30303, USA.

[2]Emory Institute for Drug Development, Emory University, Atlanta, GA 30322, USA.

[3]Virology Division, Department of Laboratory Medicine and Pathology, University of Washington Medical Center, Seattle, Washington, USA

*Corresponding author: rplemper@gsu.edu

Abstract

Orthoparamyxoviruses such as human parainfluenza virus type-3 (HPIV3), measles virus (MeV), and emerging henipaviruses pose a substantial threat to human health. We discovered an orally efficacious broad-spectrum non-nucleoside inhibitor of orthoparamyxovirus polymerases. However, here we found that tolerability in higher mammals was limited to 50 mg/kg b.i.d., close to the lowest efficacious dose. We report development of a clinical candidate analog, GHP-88310 (EIDD-3608), which combines improved oral efficacy with favorable tolerability in non-rodent species (ferrets and dogs), greatly expanding the therapeutic window. GHP-88310 had potent activity against the primary indication, HPIV3 and related respiroviruses, and the secondary indication, MeV and related morbilliviruses. In 7-day multi-dose tolerability studies, daily doses of 2,000 mg/kg were well-tolerated. Pharmacokinetic analysis revealed an altered plasma exposure profile after oral delivery of GHP-88310 compared to the original hit. In the HPIV3 cotton rat model, GHP-88310 significantly reduced viral load in the upper and lower respiratory tract when administered orally at 50 mg/kg twice daily. Therapeutic administration to ferrets infected with canine distemper virus (CDV), causing lethal measles-like disease, resulted in complete survival, significant reduction of primary viremia and shed viral load, and alleviated lymphocytopenia. Once-daily GHP-88310 was efficacious at respective 50 mg/kg and 150 mg/kg in the CDV ferret and HPIV3 cotton rat models. The compound was sterilizing against HPIV3 at pharmacokinetics-informed dynamic concentrations in disease-relevant human airway epithelium organoids. These results identify GHP-88310 as a candidate for urgently needed improved orthoparamyxovirus disease management.

21 **Introduction**

22 The orthoparamyxovirus subfamily contains major emerging and reemerging pathogens, such as
23 measles virus (MeV), the human parainfluenzaviruses type 1 and 3 (HPIV1 and HPIV3), and the highly
24 pathogenic Nipah and Hendra viruses (NiV and HeV) (*1, 2*). These viruses circulate in the human
25 population or can readily transition species barriers as exemplified by spillover of NiV from *Pteropus* fruit
26 bats to domestic animals and humans (*2*).

27 Although a live-attenuated measles vaccine has been available for decades, endemic transmission
28 of MeV continues in large geographical areas including parts of Europe. Largely fueled by reports of an
29 alleged link between the MMR vaccine and the incidence of autism (*3, 4*), measles vaccination rates have
30 declined in the last decade in the US. Further exacerbated by the COVID-19 pandemic (*5, 6*), low herd
31 immunity in 2025 resulted in the largest measles outbreak in North America in 3 decades with over 1,500
32 confirmed cases around the epicenter in West Texas, three deaths, and thousands of additional cases
33 in neighboring states, Mexico, and Canada(*7-9*). Approximately 20% of patients were hospitalized with
34 severe disease (*10*). However, no approved antivirals for improved measles management beyond
35 supportive care exist (*11-13*). A major obstacle that has hampered drug development against MeV is the
36 challenge of conducting clinical efficacy trials in a predominantly pediatric patient population (*14-16*). In
37 contrast, related HPIV3 can reinfect people throughout life. Older adults and the immunocompromised
38 are at greatest risk of HPIV3 spread to the small airways, causing lower respiratory tract infection (LRTI)
39 that presents with bronchiolitis and pneumonia (*17, 18*). Adult hematopoietic stem cell transplant
40 recipients are among the most vulnerable groups with mortality rates from HPIV3 LRI of up to 75% (*19,*
41 *20*), and no vaccine prophylaxis or therapeutic is currently available to manage the disease.

42 We have identified HPIV3 as the primary indication for an anti-orthoparamyxovirus drug development
43 program based on the rationale that the HPIVs constitute an unmet medical need with an estimated 3
44 million medically attended cases in the United States annually (*21, 22*); that progression to severe HPIV3
45 disease in at-risk adults is relatively slow with a median of 3 days between upper respiratory symptoms
46 and onset of pneumonia, opening a window for intervention (*20*); and that precedence for clinical
47 evaluation of HPIV3 inhibitors in transplant patients has been established (*19, 20*).

48 In previous work, we identified a novel non-nucleoside inhibitor class of the paramyxovirus RNA-
49 dependent RNA polymerase (RdRP) complex through an anti-HPIV3 high-throughput drug screen (*23,*
50 *24*). The hit compound, GHP-88309, showed unusually broad-spectrum sub-micromolar activity against
51 orthoparamyxoviruses of the respirovirus (HPIV1, HPIV3, Sendai virus (SeV)), morbillivirus (MeV and
52 canine distemper virus (CDV)), and henipavirus (Ghana henipavirus and Cedar virus) genera (*23-25*).
53 Mechanistic characterization revealed that GHP-88309 binding prevents initiation of the viral RdRP
54 complex at the promoter, most likely by sterically blocking structural reorganization of the polymerase
55 from initiation into elongation configuration (*23, 24, 26*). For proof-of-concept, we established oral
56 efficacy in the SeV-mouse model as a lethal substitute assay for human respirovirus disease (*23, 24*).
57 In parallel, we validated broad anti-orthoparamyxovirus efficacy in CDV-infected ferrets, which develop
58 measles-like disease that presents with high fever, rash, and lymphocytopenia (*25*). The infection
59 recapitulates severe measles cases, since CDV pathogenicity in ferrets is high and all infected animals
60 succumb within 10-12 days of infection (*25*). A course of oral GHP-88309 started after the onset of
61 clinical signs but before peak viremia changed outcome and all treated animals survived (*23, 24*). Thus,
62 GHP-88309 met three fundamental requirements of the target product profile that we require of an anti-
63 orthoparamyxovirus candidate: orally bioavailable to facilitate rapid self-administration; active against
64 different high-consequence orthoparamyxoviruses including an indication with a clear path to clinical
65 testing; and shelf-stable under ambient conditions for stockpiling and rapid distribution. However, the
66 envisioned clinical use in pediatric patients and the immunocompromised demands high tolerability with
67 wide safety margins.

68 In this study, we report an unexpected tolerability limit of GHP-88309 in higher mammals of 50
69 mg/kg. In search of a clinical candidate, we launched a synthetic lead development program that
70 yielded a novel chemotype class with favorable tolerability in rodent and non-rodent (ferrets and dogs)
71 toxicology species. We report enhanced oral efficacy of this candidate against the primary HPIV3
72 indication in a relevant animal model, show a broadened therapeutic window against the secondary
73 measles indication, and establish dosing paradigms against HPIV3 in disease-relevant human airway
74 epithelium organoid cultures based on PK-informed physiologically achievable dynamic concentrations.

75

76 **Results**

77 Prolonged 17-day treatment of CDV disease in ferrets with the first-generation lead GHP-88309
78 was highly effective at a minimally efficacious oral dose of 50 mg/kg b.i.d. and all animals survived the
79 infection (*25*). In mice, multi-dose administration of GHP-88309 at 150 mg/kg (highest dose tested)
80 b.i.d. was well tolerated without adverse events (*23*).

81 **Synthetic lead development to overcome tolerability limitations of GHP-88309**

82 To estimate the therapeutic index (TI) of GHP-88309 in a non-rodent species, we increased oral
83 dose levels to 150 mg/kg in a multi-dose PK study in search of tolerability limits in ferrets (Fig. 1A).
84 Unexpectedly, ferrets in the 150 mg/kg group reached endpoint within hours following the second dose
85 (Fig. 1B, Fig. S1A,B). Complete blood count (CBC) analysis revealed a drastic drop in platelet counts in
86 animals of this group after compound administration (Fig. S1C). Plasma PK analysis of the 50 mg/kg
87 group on day 7 (after 14 doses) showed high plasma concentration peaks (C_{max} 43.5 μM) and an
88 overall exposure of 270 μM × hr (Fig. 1C). A single ascending dose study confirmed that a dose level of
89 50 mg/kg was well tolerated, whereas animals receiving 150 mg/kg showed transient paralysis and a
90 drop in body temperature, and ferrets dosed at 500 mg/kg died within 4 hours of dosing (Fig. 1D-F).

91 Building on our initial understanding of the structure-activity relationship (SAR) of the scaffold (*23*),
92 we launched a synthetic lead development program with the primary objective to improve tolerability in
93 non-rodent species. Six azaquinoline lead candidates emerged from this exercise (Table S1), each
94 featuring a substituted heterocyclic ring (Fig. 1G). None showed appreciable cytotoxicity in cell culture
95 (Fig. 1H) and all maintained antiviral potency *in vitro* within a <2-fold range against the HPIV3 primary
96 indication (Fig. 1I) and respective <8-fold and <3-fold range against the morbillivirus (Fig. 1J) and
97 henipavirus (Fig. 1K) secondary indications.

98 Single-dose PK prescreening of these six candidates in mice at an oral dose level of 20 mg/kg
99 revealed highest plasma exposure for, in descending order, GHP-88382, GHP-88310, and GHP-88370.
100 However, none of these analogs reached the high exposure levels of GHP-88309 (Fig. 1L). Based on
101 PK performance, we selected these three analogs for proof-of-concept efficacy testing against the

102 primary respirovirus indication.

103 **GHP-88310 efficacy against the primary respirovirus indication**

104 Using the lethal SeV 129X1/SvJ mouse model as a surrogate for human respirovirus disease, we
105 screened the three developmental candidates in comparison with GHP-88309, each dosed orally at 150
106 mg/kg twice daily (b.i.d.), initiated 24 hours after infection (Fig. 2A). All animals receiving GHP-88309
107 and GHP-88310 survived without developing clinical signs, whereas GHP-88382 mediated only partial
108 survival and GHP-88370 provided no therapeutic benefit (Fig. 2B, Fig. S2A,B). Viral load in the upper
109 (Fig. 2C) and lower (Fig. 2D) respiratory tract of GHP-88310-treated animals was significantly reduced
110 compared to vehicle-treated mice. Effect size was equivalent to that achieved by GHP-88309. In
111 contrast, GHP-88382 reduced viral burden only in the lower respiratory tract and GHP-88370 had no
112 significant effect on viral load.

113 Accordingly, we selected GHP-88310 for a dose-to-failure study against the primary indication in
114 the HPIV3 cotton rat model, measuring viral load in the respiratory tract 3.5 days post-infection (dpi;
115 Fig. 2E). In this model, the minimal dose of original hit GHP-88309 that significantly reduced viral load
116 in both trachea and lungs was 300 mg/kg b.i.d. (Fig. 2F,G; Fig. S3A,B). GHP-88310 was substantially
117 more potent, showing lowest efficacious doses of 50 mg/kg b.i.d. and 16.5 mg/kg b.i.d. in the upper and
118 lower respiratory tract, respectively. Plasma exposure of GHP-88310 in cotton rats was approximately
119 one-half that of GHP-88309 after a single oral dose of 50 mg/kg, despite greater efficacy of GHP-88310
120 (Fig. 2H,I). Corresponding variations in tissue distribution were greatest in brain, heart, and kidneys,
121 smallest in liver and lung (Fig. 2J). However, none of these differences were statistically significant.

122 A 7-day ascending multi-dose study with GHP-88310 culminating in a 2,400 mg/kg daily dose (Fig.
123 2K) showed that the compound was well tolerated at all dose levels without changes in bodyweight,
124 temperature, or other adverse signs (Fig. 2L; Fig. S4A,B). Plasma exposure built up to nearly 2,000 μM
125 × hr at the highest dose (Fig. 2M). Trough plasma concentrations at the lowest dose tested exceeded
126 19 μM, corresponding to 5-times the cell-culture EC_{90} concentration of GHP-88310 against HPIV3.
127 Based on these high exposure levels, we examined anti-HPIV3 efficacy in a once-daily (q.d.)
128 therapeutic dosing regimen, starting treatment of cotton rats 12 hpi (Fig. 2N). Oral GHP-88310 at 150

129 mg/kg q.d. or higher significantly reduced viral load in trachea and the lower respiratory tract (Fig.
130 2O,P) without changes in body weight or temperature (Fig. S5A,B).

131 **GHP-88310 tolerability in non-rodent toxicology species**

132 Having validated oral efficacy of GHP-88310 against the primary indication in cotton rats, we
133 explored PK properties of the compound in ferrets in a single ascending dose oral PK study (Fig 3A). A
134 dose level of 500 mg/kg GHP-88310 was well tolerated and plasma exposure increased dose-
135 proportionally between 150 and 500 mg/kg doses (Fig. 3B). A subsequent escalating 7-day ascending
136 multi-dose tolerability study in ferrets demonstrated that administering GHP-88310 at a daily dose of up
137 to 2,000 mg/ml (Fig. 3C) had no negative effect on bodyweight, body temperature, and CBC
138 parameters including platelet counts (Fig. S6A-E). All animals survived the full 7-day course without
139 signs of adverse effects, in contrast to reference animals dosed with GHP-88309 at 150 mg/kg, which
140 succumbed within hours of receiving the second dose (Fig. 3D). Plasma concentrations examined
141 once-daily 4 hours after dosing (expected C_{max}) plateaued dose-dependently after administration of four
142 (500 mg/kg) to eight (1,000 mg/kg) doses (Fig. 3E). Overall exposure after 7 days (14 doses) increased
143 dose-dependently from 336 μM $\times$ hr (50 mg/kg b.i.d.) to 2,140 μM $\times$ hr (500 mg/kg b.i.d) (Fig. 3F). At a
144 dose of 50 mg/kg b.i.d., total plasma exposure of GHP-88310 was slightly higher than that of GHP-
145 88309 with 336 μM $\times$ hours versus 270 μM $\times$ hours at study end (Fig. 1C vs Fig. 3F).

146 CBC parameters of GHP-88310-treated animals did not deviate from the normal range over the
147 course of the study (Fig. 3G) and whole blood chemistry panels taken on days 2 and 7 were likewise
148 unremarkable (Fig. S7). In contrast, a reference animal that had received two doses of GHP-88309 at
149 150 mg/kg showed changes in three of four liver enzymes examined – alkaline phosphatase (ALP),
150 alanine transaminase (ALT), and aspartate aminotransferase (AST) – by more than 750% one day
151 post-dosing and prior to death, suggesting GHP-88309-induced hepatotoxicity. Due to rapid death after
152 repeated administration of GHP-88309 at this dose level, a comprehensive blood chemistry analysis of
153 all animals in the reference group was not possible.

154 Based on greatly improved tolerability of GHP-88310 compared to GHP-88309, we advanced the
155 compound to single ascending-dose PK testing in beagle dogs, the predominant non-rodent toxicology

156 species used to inform investigational new drug (IND)-enabling safety studies (Fig. 3H). Dogs were
157 dosed orally with GHP-88310 at 50, 150, or 500 mg/kg, each followed by assessment of plasma
158 exposure over a 24-hour period (Fig. 3H). All dose levels were well tolerated without adverse signs or
159 weight loss of the animals (Fig. 3I). Plasma exposure ranged from 135 to 2,150 μM $\times$ hr (Fig. 3J),
160 demonstrating approximate dose-proportionality and exceeding at high-dose that observed in ferrets.
161 These results demonstrated that GHP-88310 plasma exposure levels exceeding those at which GHP-
162 88309 was lethal in ferrets were well tolerated in both ferrets and dogs (Fig. 3B and 3J).

163 **GHP-88310 efficacy against measles-like disease in ferrets**

164 Measles has emerged as an urgent secondary indication for GHP class paramyxovirus inhibitors
165 due to growing vaccination hesitancy in many high-income countries and endemic MeV transmission in
166 large geographical regions in sub-Saharan Africa and Southeast Asia (*12, 27, 28*). We have
167 demonstrated potent oral efficacy of GHP-88309 against the CDV/ferret surrogate model of human
168 measles (*25*). GHP-88310 and GHP-88309 had virtually identical antiviral activity against both MeV
169 (Fig. 1J) and CDV (Fig. 4A) in cell culture, returning active (EC_{50}) concentrations within a 2-fold range
170 of each other.

171 In a proof-of-concept oral efficacy study, we infected ferrets with a lethal inoculum of the wild type
172 CDV-5804p strain and initiated treatment at 3 dpi, when PBMC-associated viremia and fever become
173 first detectable in this model (Fig. 4B and Fig. S8A,B). Exploring two distinct treatment regimens,
174 animals received GHP-88310 either at 50 and 150 mg/kg b.i.d., or 50 and 100 mg/kg q.d., the latter
175 corresponding to the lowest efficacious daily dose of 100 mg/kg of GHP-88309 (*25*) and half that dose.
176 Treatment was continued in all groups until 10 dpi (150 mg/kg b.i.d. group) or 21 dpi (50 mg/kg b.i.d.
177 and q.d. groups). All treated animals survived the infection (Fig. 4C) and clinical signs were fully
178 mitigated (Fig. S8A,B), whereas all animals in a vehicle-treated reference group succumbed to CDV
179 disease with a median survival of 11 dpi. Cell-associated viremia was first detectable 3 dpi, when
180 therapeutic treatment was initiated, and rapidly progressed in vehicle-treated animals to peak viremia
181 titers of approximately 1.3×10^5 $TCID_{50}$ units per 10^6 PBMCs at 7 dpi (Fig. 4D). Treatment at 50 or 100
182 mg/kg q.d. or 50 mg/kg b.i.d. lowered peak titers by ~1 order of magnitude and resolved viremia with

183 similar kinetics by 15-16 dpi. Treatment at 150 mg/kg reduced peak viremia by 2 orders of magnitude
184 and was sterilizing at 10 dpi. The effect of treatment on shed virus load in nasal lavages closely
185 mirrored that on viremia titers (Fig. 4E). Virus shedding from animals receiving GHP-88310 at 150
186 mg/kg b.i.d. peaked 2 orders of magnitude lower than in the vehicle group and shedding from treated
187 animals ceased 6 dpi. Low b.i.d. dose animals and animals of both q.d. groups showed biphasic
188 shedding kinetics, characterized by an initial decline after treatment start followed by a second
189 shedding peak at approximately 10 dpi. Infectious virus was undetectable in all treated animals 17 dpi.
190 Lymphocytopenia, a hallmark of morbillivirus disease, was efficiently mitigated by 50 mg/kg b.i.d. or 100
191 mg/kg q.d. GHP-88310 and fully suppressed at the 150 mg/kg b.i.d. dose level (Fig. 4F). Animals in the
192 50 mg/kg q.d. treatment group experienced vehicle-like lymphocytopenia until 9 dpi. Subsequently,
193 lymphocyte counts rapidly stabilized and returned to normal range by 27 dpi. Consistent with transient
194 lymphocytopenia, the emergence of neutralizing antibodies was delayed in animals of the 50 mg/kg q.d.
195 cohort compared to the other treatment groups (Fig. 4G). Whole genome sequencing of treatment-
196 experienced virus populations recovered from animals 3, 5, 8,13, and 14 dpi did not detect any
197 mutations in polymerase proteins (supplementary dataset file S1), indicating a high barrier against viral
198 escape from GHP-88310 *in vivo*.

199 **Molecular interactions between GHP-88310 and the viral L protein**

200 We have identified the central cavity of the viral P-L polymerase complex as target site for GHP-
201 88309-class inhibitors through photo-affinity crosslinking and reduced susceptibility profiling (*23*).
202 Several high-resolution structural models of the MeV polymerase complex were recently solved (*29,*
203 *30*), setting the stage for extraction of the GHP-88310 docking pose. Activity testing of GHP-88310
204 against panels of recombinant HPIV3 (Fig. 5A), recombinant SeV (Fig. 5B), and MeV minigenome (Fig.
205 5C) harboring mutations mediating escape from GHP-88309 demonstrated, with few exceptions, high
206 consistency of resistance sites, suggesting conserved docking poses of both compounds. We defined
207 substitutions that caused a >5-fold increase in EC_{50} and/or EC_{90} values as major drivers of reduced
208 viral susceptibility (highlighted in Fig. 5A-C). Exceptions were the HPIV3 L-T1010A variant, which
209 remained fully sensitive to GHP-88310, and SeV L-Y942H, which mediated robust resistance to GHP-

210 88310 but moderate escape from GHP-88309.

211 Informed by these conserved mediators of resistance and photoaffinity mapping results for GHP-
212 88309, we docked both compounds *in silico* into a native structural model of the MeV polymerase
213 (PDB: 9DUS). Top scoring poses consistently placed both inhibitors into the same defined pocket at the
214 interface between the L protein RdRP and PRNTase domains (Fig. 5D and Fig. S9). However, distinct
215 predicted docking poses emphasized a high-affinity interaction between the GHP-88310 diazo quinoline
216 ring and residue A866 of the RdRP domain that was not present in the GHP-88309 pose (Fig. S10A,B).
217 Major resistance sites lined the binding pocket, predicting direct contact between the ligand and L-
218 protein residues A866, Y942, and T1010. Additional hot-spot sites were located in close proximity,
219 suggesting that viral escape from either inhibitor is predominantly due to primary, rather than long-
220 range secondary, resistance.

221 **GHP-88310 efficacy in primary human cells and organoids**

222 To assess whether antiviral potency of GHP-88310 supports realistic human dose concentrations,
223 we determined efficacy in physiologically relevant primary human airway epithelium cells and well-
224 differentiated human airway epithelium organoids. Wash-in and wash-out studies assessed intracellular
225 exposure levels during 2-hour periods in undifferentiated human bronchial tracheal epithelial cells
226 (HBTECs) in, respectively, the presence of 80 μM extracellular GHP-88310 (wash-in) or after removal
227 of extracellular compound (wash-out) (Fig. S11). At wash-in, a maximal intracellular exposure plateau
228 of approximately 10^5 pmol/10^6 cells was reached in 15 minutes (earliest sampling time point), indicating
229 high plasma-membrane permeability, and was sustained for the duration of the experiment. After
230 removal of extracellular GHP-88310, intracellular drug levels declined by approximately 2 orders of
231 magnitude within the 2-hour monitoring window.

232 Efficacy testing of GHP-88310 against the primary HPIV3 indication in undifferentiated HBTECs
233 showed sub-micromolar potency and a steep Hill slope, resulting in a fully sterilizing antiviral effect at
234 concentrations of 10 μM and greater (Fig. 6A). After generation of well-differentiated airway epithelium
235 organoids grown at air-liquid interface (Figure 6B), we exposed cultures to ascending concentrations of
236 GHP-88310 in the basolateral chamber of the transwell system for 48 hours each and measured

237 corresponding transepithelial electrical resistance (TEER) as a well-established marker of cytotoxicity in
238 the system(*31-33*). Electrical resistance remained unchanged at approximately 600 ohm × cm^2 before
239 and after exposure (Fig. 6C), indicating that GHP-88310 was well-tolerated at the highest
240 physiologically achievable concentrations without disturbing tissue integrity.

241 Dose-response assays using static concentrations of basolateral GHP-88310 after apical infection
242 of organoids with 5,000 plaque forming units (pfu) HPIV3 returned nanomolar EC_{50} values with
243 favorable hill slope (EC_{90} 0.13 μM), based on titers of apically released progeny virions (Fig. 6D).
244 Sterilizing conditions were reached at 1.85 μM GHP-88310 in the basolateral chamber, approximately
245 equivalent to trough plasma concentrations in the multi-dose ferret PK studies when compound was
246 administered at 50 mg/kg. To verify enhanced antiviral potency of HPIV3 in the organoid models
247 compared to immortalized cell lines, we imaged HPIV3-infected, fixed, and stained organoid sections
248 after incubation in the presence of 0.5 or 10 μM compound. Titration of progeny virions prior to imaging
249 demonstrated that 0.5 μM basolateral GHP-88310 reduced virus titers by approximately 2 orders of
250 magnitude (Fig. 6E), which was consistent with the dose-response assay results. Anti-ZO-1 staining
251 revealed an unperturbed tight junction network in the presence of both concentrations examined,
252 similar to mock-treated uninfected cultures (Fig. 6F). Only sporadic viral antigen was detectable after
253 incubation of infected cells in the presence of 0.5 μM GHP-88310, and none after incubation with 10
254 μM compound, whereas HPIV3 proteins were abundant in organoids that had received vehicle volume-
255 equivalents. Overlay of viral and beta-actin stains revealed that viral replication was concentrated in
256 ciliated cells (Fig. S12), consistent with previous reports for HPIV3(*34, 35*).

257 To assess GHP-88310 efficacy in human organoids at physiological, dynamic concentrations, we
258 recapitulated ferret plasma PK curves in the basolateral chambers of the airway epithelium organoids
259 infected with HPIV3. Two dose levels, 20 mg/kg and 50 mg/kg, each represented by b.i.d. and q.d.
260 dosing regimens, were simulated over a 48-hour period each (Fig. 6G). At study end, we determined
261 progeny virus yields released from the apical surface. Validating our finding of high anti-HPIV3 potency
262 of static GHP-88310 in the organoids, both high-dose regimens were sterilizing (Fig. 6H). Also
263 simulating a low-dose b.i.d. treatment fully suppressed production of infectious progeny virions (Fig. 6I),

264 although plasma PK profiles called for peak GHP-88310 concentrations of only ~15 μM and no
265 compound was present in the basolateral chamber for 6 hours in every 12-hour interval (Fig. 6H). Even
266 recapitulating a 20 mg/kg q.d. plasma exposure profile in the basolateral chamber, which comprised
267 compound-free incubation periods of 18 hours in every 24-hour interval, greatly inhibited virus
268 replication. Progeny virus yield was statistically significantly reduced by over two orders of magnitude
269 compared to organoid cultures that had been incubated in the presence of basolateral vehicle volume-
270 equivalents (Fig. 6I). These results support high developmental potential of GHP-88310 for human
271 therapy, demonstrating that potent antiviral efficacy is achieved at physiological concentrations in
272 disease-relevant human tissue models without cytotoxicity limitations.
273

274 **Discussion**

275 This study identified the broad-spectrum anti-orthoparamyxovirus clinical candidate GHP-88310,
276 which showed favorable tolerability properties in rodent species and higher mammals including dogs. De-
277 risking GHP-88309 illuminated a sharp tolerability limit in higher mammals at concentrations exceeding
278 100 mg/kg daily dose. We addressed this issue synthetically through development of GHP-88310, which
279 occupies novel chemical space and was tolerated without adverse effects by ferrets and dogs at very
280 high dose levels that far exceeded the lethal dose of GHP-88309 in ferrets. Differential responses
281 between rodents and non-rodents to drug exposure are not unusual and often attributable to the high
282 metabolic rate of rodents(*36-38*), an expanded rodent cytochrome P450 system that results in fast
283 breakdown of drugs with frequently distinct metabolites (*39-41*), and/or the high liver to body weight ratio
284 of rodents that increases resistance to chemical stress (*42*). In the case of GHP-88309, plasma exposure
285 was high after oral dosing in both rodents and non-rodents, but only non-rodents experienced tolerability
286 limits. At equal dose levels, GHP-88310 exposure trailed that of GHP-88309. Our ascending dose PK
287 studies demonstrated, however, that improved tolerability of GHP-88310 was not a trivial consequence
288 of lower exposure compared to GHP-88309, since plasma exposure in ferrets and dogs after high-dose
289 GHP-88310 far exceeded lethal levels of GHP-88309 in ferrets. We propose that toxicity of high-dose
290 GHP-88309 in non-rodents results most likely from accumulation of an unidentified metabolite, which is

291 not produced in rodents due to their distinct cytochrome P450 composition, and absent from GHP-88310
292 breakdown products due to its distinct chemical structure.

293 A hallmark of viral escape from GHP-88309 is that resistance emerged readily in cell culture, but all
294 escape variants were apathogenic and no escape mutations appeared *in vivo* (*23*). Susceptibility
295 testing of developmental candidate GHP-88310 against recombinant strains of three viral targets – the
296 primary indication HPIV3, surrogate respirovirus SeV, and secondary indication MeV – that each
297 harbored confirmed GHP-88309 escape mutations (*23*) revealed overlapping susceptibility profiles. All
298 mutations were located in the viral L protein, lining the interface between the RdRP and PRNTase
299 domains in the central polymerase cavity. However, tolerance to GHP-88310 was, in most cases, less
300 robust than escape from GHP-88309. Conserved susceptibility profiles spotlight a common molecular
301 target site of both compounds, whereas reduced robustness of escape from GHP-88310 suggests
302 altered docking poses, which was substantiated by *in silico* QSAR models. Importantly, this hallmark
303 feature of GHP-88309 resistance appears to equally apply to GHP-88310, since whole genome
304 sequencing of heavily treatment-experienced virus populations recovered from ferrets did not reveal
305 substitutions at known escape hot-spots or any other polymerase residues. Although future work must
306 address whether additional specific GHP-88310 escape sites exist, our results indicate a high barrier
307 against viral escape from GHP compounds without concomitant loss in pathogenicity.

308 It was the primary focus of this synthetic lead identification program to improve tolerability in higher
309 mammals without compromising antiviral potency, and GHP-88309 and GHP-88310 indeed have equal
310 activity in cell culture. We therefore did not anticipate also achieving a substantial *in vivo* potency boost
311 in both rodent and non-rodent host species. Quantitation of drug tissue levels of both compounds in
312 cotton rats excluded improved lung tissue distribution of GHP-88310 as a possible explanation for this
313 approximately 6-fold increase in antiviral efficacy. Whereas the lowest efficacious dose of GHP-88309
314 and GHP-88310 in the CDV ferret model was the same (50 mg/kg), plasma exposure of GHP-88310
315 was lower than that achieved by GHP-88309 after equal doses. The conclusion of an *in vivo* potency
316 boost in both models was further supported by our observation that GHP-88310 was efficacious also in
317 a q.d. regimen, lowering the minimally required efficacious daily dose by 50%. We propose that

318 breakdown of GHP-88310 in both rodents and non-rodents may generate a bioactive, but non-toxic,
319 metabolite that carries part of the antiviral efficacy, whereas GHP-88309 metabolism produces a toxic
320 by-product. Both effects, increased tolerability and enhanced antiviral efficacy of GHP-88310, have
321 substantially expanded the therapeutic window of the compound against the primary and secondary
322 indication in relevant animal models, underscoring high clinical potential.

323 *Ex vivo*, potency of GHP-88309 against HPIV3 in established cell lines and primary HBTECs was
324 virtually identical. However, we noted an approximately 5-fold higher antiviral potency in disease-
325 relevant, well-differentiated human airway epithelium organoids versus the undifferentiated HBTECs.
326 This effect may be due to a combination of the diverse cell types present in the organoids, their
327 complex 3D-architecture, and the more natural nutrient concentration gradient compared to simple cell
328 monolayers (*43-46*). Indeed, confocal microscopy identified, consistent with previous reports (*34, 35*),
329 ciliated cells as the primary host cell type for HPIV3 replication in the airway epithelium cultures. To test
330 the correlation between oral dose level and antiviral effect, we recapitulated ferret PK-informed dynamic
331 compound concentrations in the basolateral chamber of the transwell cultures, simulating repeat oral
332 dosing ranging from 20 mg/kg q.d. to 50 mg/kg b.i.d. We first implemented this approach when
333 developing molnupiravir (*47*). Simulating plasma concentrations of a 20 mg/kg q.d. GHP-88310 dosing
334 regimen in the basolateral chamber significantly reduced progeny virus yields by several orders of
335 magnitude, which translates under consideration of established species conversion factors (*48*) to a
336 feasible predicted oral human dose target as low as 200 mg daily. Corroborating these results, higher
337 dose levels were fully sterilizing.

338 Simulation of 20 mg/kg b.i.d. or 20 mg/kg q.d. regimens entailed two 6-hour or one 18-hour
339 window, respectively, in every 24-hour period in which no compound was present in the basolateral
340 chamber. Effective viral inhibition despite prolonged incubation in the absence of inhibitor is likely due
341 to inhibition of both replicase and transcriptase activity of the viral polymerase complex by GHP class
342 compounds (*26, 49*). This concerted action may arrest the viral replication cycle in the primary
343 transcription stage (*49*), preventing exponential expansion of viral protein expression and suppressing
344 production of immune-modulatory viral V and C proteins that counteract the type I host interferon

345 response (*50-53*), which exposes the virus to host cells in an unmitigated antiviral state. Both the
346 HPIV3 cotton rat and CDV ferret models confirmed that effective virus inhibition by only intermittently
347 present GHP-88310 was not an artifact of the *ex vivo* organoid system, since q.d. administration of
348 GHP-88310 at the lowest efficacious dose likewise resulted in either model in prolonged periods with
349 undetectable plasma drug levels. These results thus establish proof-of-concept that efficacious
350 orthoparamyxovirus therapy with a non-nucleoside polymerase inhibitor does not depend on continuous
351 drug plasma concentrations above the minimum inhibitory level, illuminating an overproportional
352 beneficial effect of targeting the mononegavirus polymerase complex.

353 Naturally, human organoid systems can only partially simulate the complexity of human infection.
354 Whereas first-in-human dose levels will be determined based on toxicology results, the organoids
355 provide valuable insight into defining desirable dosing objectives. Other limitations of our study arise
356 from incomplete recapitulation of all aspects of human disease presentation by animal models,
357 currently undefined highest tolerated dose levels of GHP-88310, and limited insight into a possible
358 effect of co-morbidities and/or low patient immune competence on antiviral efficacy. However, ferrets
359 are a natural host for CDV and hallmarks of human morbillivirus disease are fully preserved, supporting
360 confidence that treatment paradigms established in this model will provide valuable guidance for
361 performance in human therapy. In summary, this study identified a much-needed novel developmental
362 candidate for treatment of orthoparamyxovirus infections that combines attractive drug-like properties
363 with potent antiviral efficacy and unusually broad indication spectrum, opening a viable path to clinical
364 testing.

365

366 **Material and Methods**

367 **Study design**

368 Cells, normal human bronchial/tracheal epithelial (NHBE) cells, well-differentiated air liquid
369 interface (ALI) human airway epithelial (HAE) cells, ferrets, cotton rats and mice were used as models
370 to examine the efficacy of GHP-88310 and other GHP-88309 analogs against HPIV3, SeV, and CDV.
371 Viruses were administered through intranasal inoculation and virus load was monitored continuously in

372 nasal lavages (ferrets only), and in respiratory tissues of cotton rats and mice extracted when indicated
373 after infection. Virus titers were determined through $TCID_{50}$-titration/ plaque assays.

374 **Cells, viruses, and compound synthesis**

375 Vero E6, Vero E6 TMPRSS2, Vero cells stably expressing canine signaling lymphocyte activation
376 molecule (Vero c-SLAM, VDS), Vero-hSLAM, and BHK-T7 cells (BHK cells stably expressing T7) were
377 cultured in Dulbecco's modified Eagle's medium (DMEM) supplemented with 7.5% heat-inactivated
378 fetal bovine serum (FBS) at 37°C and 5% CO_2. Cells were tested regularly for mycoplasma
379 contamination prior to usage. Recombinant SeV-GFP, rCDV 5804p, HPIV3 (clinical isolate 13J5,
380 HPIV3/Seattle/USA/13J5/2016; KY629774.1), rPIV3-nano (JS strain), rMeV (Edmonston strain), and
381 rCedar virus (CedV)-nano were propagated on Vero E6 TMPRSS2 or VDS cells using DMEM with
382 7.5% serum, scraped when necessary, clarified, aliquoted, and stored at −80°C. The generation of all
383 GHP-88309 resistant recombinant viruses used in these studies has been previously described (*23*).
384 Virus stock titers were determined through $TCID_{50}$-titration (rSeV, rCDV, rMeV, and rCedV) or plaque
385 assay (PIV3), and stocks were stored in aliquots at -80°C. All virus stocks were sequence confirmed
386 prior to usage. GHP-88310 and other GHP-88309 analogs were authenticated through elemental
387 analysis (Table S1) and stored as dry powder (supplementary information. Working aliquots were
388 dissolved in DMSO or 1% methylcellulose for *in vitro* and *in vivo* studies, respectively.

389 **Primary cells**

390 Undifferentiated cells: Normal human bronchial/tracheal epithelial cells (Lonza CC-2540S, lot
391 number 519670, Caucasian, 42-year-old female donor "F3", unknown cause of death, smoker) were
392 amplified and expanded in lifeline cell culture media (LIFELINE Cell Technology) for no more than 3
393 passages. Cells were seeded in 24-well plates for experiments.

394 Differentiated ALI HAE cells (MatTek): EpiAirways (AIR-100; 23-year-old healthy male, Caucasian;
395 grown at air-liquid interface for 13 days) were equilibrated after arrival and further differentiated in
396 hanging-top plates (following manufacturers protocol) for 14-21 days prior to use in experiments. ALI
397 HAE cells were fed every two days 6 ml maintenance media (MatTek), rinsed weekly and before a
398 procedure (MatTek, TEER buffer). Transepithelial/transendothelial electrical resistance (TEER) was

399 measured on selected inserts using an EVOM3 (World Precision Instruments) following manufacturers
400 protocol.

401 **Virus titration**

402 $TCID_{50}$: Samples were serially diluted (10-fold starting at 1:10 initial dilution) in serum-free DMEM.
403 Serial dilutions were added to either VDS (rCDV), Vero hSLAM (rMeV), BHKT7 (rCedV), or Vero E6
404 TMPRSS2 (rSeV) cells seeded in 96-well plates at 1×10^5 cells/ml, 14 hours before infection. Infected
405 plates were incubated for 72-96 hours at 37°C with 5% CO_2, and titers were determined (Reed and
406 Muench).

407 Plaque assays: HPIV3 virus samples were serially diluted (10-fold starting at 1:10 initial dilution) in
408 serum-free DMEM. Serial dilutions were added to Vero E6 TMPRSS2 cells seeded in 12-well plates at
409 2×10^5 cells per well, 20 hours before infection. Ninety minutes post infection, cells were overlaid with 1
410 ml of 2× DMEM and avicel (1:1 ratio). Infected plates were incubated for 84 hours at 37°C with 5% CO_2.
411 Upon incubation, cells were washed twice with PBS, stained with 1% crystal violet (in 20% EtOH), and
412 plaques were enumerated.

413 **Dose-response and minigenome antiviral assays and cytotoxicity assessment**

414 Compound stocks were prepared in dimethyl sulfoxide (DMSO) and diluted in cell culture media
415 (final DMSO concentration of less than 0.1% in all wells). For luciferase-based dose-response assays,
416 cells were seeded in white-walled 96-well plates one day prior to the experiment to achieve 50%
417 confluency. Threefold serial dilutions of compounds were prepared in triplicate using an automated
418 Nimbus liquid handler (Hamilton) and transferred to the cells. Immediately after the addition of
419 compound, cells were infected with virus as previously described (*54*). Each plate contained four wells
420 of positive and negative control (media containing 100 μM cycloheximide or vehicle (DMSO),
421 respectively). Luciferase activities were determined 48 hours after infection using Nano-GLO buffer
422 (Promega) and an H1 Synergy plate reader (Biotek). Normalized luciferase activities were analyzed
423 with the following formula: % inhibition = $(Signal_{sample} - Signal_{min})/(Signal_{max} - Signal_{min}) \times 100$, and
424 dose-response curves were further analyzed by normalized nonlinear regression with variable hill slope
425 to determine EC_{50} and EC_{90}.

426 BSR-T7/5 cells (5 × 10^4 per well in a 96-well plate format) were transfected with plasmids encoding
427 for P-ICB (0.01 μg), N-ICB (0.01 μg), L-ICB (0.0075 μg) and L-ICB mutant variants (0.0125 μg), and the
428 MeV luciferase replicon reporter (0.02 μg) using GeneJuice transfection reagent. Cells were lysed 42
429 hours after transfection with OneGlo substrate (Promega), which was directly added to the cells, and
430 bioluminescence was quantified using the above-mentioned formula.

431 Virus yield reduction assays with CDV and SeV: Cells were seeded in 24-well plates. Once
432 reaching 90% confluency, cells were overlaid with compound dilutions (three-fold dilutions, in triplicate)
433 and cells were infected at an MOI of 0.1. CDV: After 28 hours of incubation, the supernatant was
434 removed, and cells were scraped in 300 µl media, subjected to two freeze-thaw cycles, clarified, and
435 the resulting supernatant was collected for titration. SeV: Supernatant was collected after 52 hours and
436 clarified. Samples were titrated and scored using the $TCID_{50}$ method after 4 days.

437 Virus yield reduction assays in undifferentiated NHBE cells: Cells were seeded at 60% confluency
438 in a 24-well plate. Upon reaching 80% confluency, cells were overlaid with compound dilutions (50 µM,
439 three-fold dilutions, in triplicate) and were infected at an MOI of 0.1 with HPIV3 (clinical isolate 13J5).
440 Supernatant was collected after 48 hours and clarified. Samples were titrated by plaque assay on Vero
441 E6 TMPRSS2 cells and quantified after 4 days.

442 Virus yield reduction assays in EpiAirways: Inserts were rinsed using DPBS and infected on the
443 apical side with 10,000 PFU of HPIV3 (clinical isolate 13J5) per well in 100 µl PBS. Sixty minutes after
444 infection, virus was aspirated to allow for air-liquid exchange. Compound dilutions (50 µM, three-fold
445 dilutions, in triplicate) were added on the basolateral side at the time of infection and ALI HAE cells
446 were incubated for 48 hours (after 24 hours, the basolateral media was exchanged - same static
447 compound concentration). After 20 hours of initial incubation, the apical surface was washed once to
448 remove accumulated mucus. Apical shed was harvested in 300 µl PBS that had been incubated at
449 37°C for 30 min. Clarified samples were titrated by plaque assay on Vero E6 TMPRSS2 cells and
450 measured after 4 days.

451 To assess the impact of the GHP-compound class on cell metabolic activity, Vero E6 cells were
452 seeded at 6,000 cells per well in a 96-well plate and incubated at 37°C (5% CO_2) following the addition

453 of a 3-fold serial dilution of each compound, starting at 150 μM. After 72 hours of incubation, cells were
454 incubated with 10 μl per well of PrestoBlue (ThermoFisher Scientific) for 1 hour at 37°C and
455 fluorescence was measured using an H1 synergy plate reader (Biotek) with excitation and emission
456 wavelengths set at 560 nm and 590 nm, respectively. Cellular metabolic activity as a surrogate for cell
457 viability was expressed as a percentage relative to the media control.

458 To determine the effect of GHP-88310 on cell metabolic activity in primary cells, three to four ALI
459 HAE cultures were exposed to increasing concentrations of GHP-88310 (25 μM - 200 μM) in
460 maintenance media (MatTek). To assess barrier integrity, TEER was measured after 48 hours of
461 incubation at 37°C with 5% CO_2 and immediately prior to compound addition to the basolateral
462 chamber of a 12-well hanging insert plate (MatTek). The measurements are displayed in Ohm $\times$ cm^2.

463 **Confocal microscopy**

464 PIV3- and mock-infected ALI HAE cells were infected and treated with GHP-88310 at either 0.5
465 μM or 10 μM as above. Forty-eight hours after infection the apical shed was harvested, and the cells
466 were prepared for confocal microscopy. All incubation steps of immunostaining were performed at room
467 temperature and in the absence of light as previously described (*47*). Briefly, the inserts were fixed for
468 40 min with 4% paraformaldehyde-PBS, washed once with PBS, cut, and mounted on a chamber slide
469 (Fisher, cat# 154461PK). Cells were permeabilized with 500 μl of 0.5% Triton X-100 in PBS for 2 hours,
470 then washed, and blocked with 500 μl per insert of 5% BSA in PBS containing 0.05% Tween-20 for 1
471 hour. Inserts were washed and stained with the primary antibody in an antibody-binding solution (2%
472 BSA-PBS) for 1 hour (PIV3: goat anti-HPIV3 HN, Abcam ab28584; TJ: mouse anti-ZO-1 BD,
473 Biosciences 610966; Mucin/Goblet cells: mouse anti-MUC5AC, ThermoFisher MA5-12175). Cells were
474 washed three times and incubated with a conjugated antibody for 45 min (donkey anti-goat Alexa Fluor
475 568 ThermoFisher A-11057; goat anti-mouse IgG (H+L) highly cross-adsorbed secondary antibody,
476 Alexa Fluor 488, Invitrogen, A-11029). Cells were washed an additional three times in PBS and then
477 incubated for 5 min with Hoechst 34580. Following three additional washes, cells were mounted with
478 coverslips using a drop of ProLong™ Diamond Antifade Reagent (Thermo Scientific, Cat# P36970) and
479 stored overnight.

480 Confocal Imaging was performed using the Zeiss Axio Observer Z.1 and an LSM 800 confocal
481 microscope with AiryScan, controlled by the Zeiss Zen 3.1 Blue software (Windows 10). This software
482 as well as Adobe Photoshop (25.9.0) were employed for image analysis.

483 **Single-dose pharmacokinetic property profiling in mice, cotton rats, ferrets, and dogs**

484 Mice: Eight-week-old female Balb/cJ mice (The Jackson Laboratory) were acclimated for at least
485 three days prior to study initiation. Mice were weighed and administered 20 mg/kg of GHP-class
486 compounds by oral gavage in 1% methylcellulose (200 µl total volume). Blood samples (150 µl) were
487 collected retro-orbitally at designated time points post dosing, centrifuged at 2,000 rpm for 5 minutes at
488 4°C, and the resulting plasma was stored at -80°C.

489 Cotton rats: Female cotton rats (Envigo), aged 2-3 months, were rested for at least three days prior
490 to study start. Animals were weighed and dosed via oral gavage with 50 mg/kg of GHP-88309 or GHP-
491 88310, formulated in 1% methylcellulose (500 µl total volume). Blood samples (150 µl) were collected
492 at 30 minutes, and at 1, 2, 3, 4 and 8 hours post dosing. Plasma was processed as described above. At
493 8 hours post-dosing, organs (lung, brain, spleen, heart, kidney, small intestine, large intestine, and liver)
494 were harvested and immediately frozen in liquid nitrogen.

495 Ferrets: Female ferrets (Triple F Farm), 4-8 months of age, were acclimated for a minimum of three
496 days prior to dosing. Animals were weighed and administered GHP-88309 or GHP-88310 via oral
497 gavage at doses of 150 mg/kg (GHP-88309) and 150 or 500 mg/kg (GHP-88310). Both compounds
498 were prepared in 1% methylcellulose, with a final gavage volume of 2 ml. Blood samples (200 µl) were
499 collected at 0.5, 1, 2, 3, 4, 6, 8, 12, and 24 hours post-dose and processed as described previously.

500 Dogs: Male and female beagles, aged 10-12 months old, were weighed and administered GHP-
501 88310 orally at 50, 150, or 500 mg/kg, formulated in 1% methylcellulose (study conducted by SRI
502 Biosciences™). Blood samples (300 µl) were collected at pre-dose, 0.5, 1, 2, 4, 6, 8, 12, and 24 hours
503 post-dosing for analysis. Clinical observations were conducted at pre-dose, immediately after dosing, 2-
504 4 hours post-dose, and again at 24 hours. The same four animals were used across all dose levels,
505 with a minimum washout period of seven days between each dose escalation.

506 For analysis, aliquots of animal plasma were mixed with 70% acetonitrile in water that included an
507 internal standard. Samples were then vortexed for one minute and collected at 15,000 rpm for 5
508 minutes. The resulting supernatants were transferred to HPLC vials for analysis by LC-MS/MS at 4°C.
509 HPLC separation was performed on an Agilent 1260 system (Agilent Technologies, Santa Clara, CA,
510 USA) equipped with an autosampler, column oven, UV lamp, and binary pump.

511 For the mouse PK study screening, a Zorbax SB-Phenyl (50x4.6mm, 3.5 µm) column (Waters) was
512 used. Mobile phase A consisted of 20 mM ammonium formate and mobile phase B consisted of
513 acetonitrile. A 2-minute isocratic HPLC method was used at 40% mobile phase A. For the remaining PK
514 studies, an XTerra MS C18 (50x2.1mm, 5 µm) column (Waters) was used. Mobile phase A consisted of
515 25 mM ammonium bicarbonate in HPLC grade water pH adjusted to 9.8 and mobile phase B consisted
516 of acetonitrile. A 2-minute isocratic HPLC method was used at 75 or 80% mobile phase A. MS analysis
517 was performed on a QTrap 7500 or Triple 7500 Mass Spectrometer (Sciex, Framingham, MA, USA) or
518 using positive electrospray ionization (ESI) in multiple reaction monitoring (MRM) mode. Data analysis
519 was performed using SciexOS Software (Sciex). PK parameters were calculated using Phoenix
520 WinNonLin 8.4 (Build 8.4.2.6172; Certara, Princeton, NJ) using the non-compartmental analysis tool.

521 Samples of frozen animal tissue were homogenized with 4°C 70% acetonitrile in water that
522 included an internal standard. Homogenate were collected for 5 minutes at 10,000 rpm and
523 supernatants subjected to a second clearance step (5 minutes, 15,000 rpm). The remaining
524 supernatant was analyzed via LC/MS/MS, maintaining samples at 4°C. HPLC separation was
525 performed on an Agilent 1260 system (Agilent Technologies) equipped with an autosampler, column
526 oven, UV lamp, and binary pump, using an Xterra MS C18 (50 x 2.1 mm, 5 µm) column (Waters).
527 Mobile phase A consisted of 25 mM ammonium bicarbonate buffer in HPLC grade water, pH 9.8, and
528 mobile phase B consisted of acetonitrile. A 4.5-minute gradient HPLC method was performed to
529 separate the analytes beginning with a 1-minute isocratic hold at 10% B, followed by a 2-minute
530 gradient to 30% B, and a return to starting conditions for 1.5 minutes. MS analysis was performed on a
531 ZenoTOF 7600 Mass Spectrometer (Sciex) using positive ESI in multiple reaction monitoring (MRM)
532 mode. Data analysis was performed using SciexOS Software (Sciex).

533 **Single-dose GHP-88309 tolerability in ferrets**

534 Female ferrets (Triple F Farm), between 6-8 months old, were acclimated for at least three days.
535 Ferrets were weighed and dosed with GHP-88309 once via oral gavage at doses ranging from 50-
536 1,000mg/kg. The compound was formulated in 1% methylcellulose and a final gavage volume of 2 ml
537 was administered. Rectal temperature and clinical scores were measured before dosing and at 30
538 minutes, as well as 1, 2, 3, 4, 5, 6, 8, 12, and 24 hours post-dose.

539 Clinical scoring evaluated: i) temperature to monitor hypothermia and ii) neurological status to
540 detect signs of acute drug toxicity. Temperature scoring was assigned as follows: 0, >38°C; 1, 37.5-
541 37.9°C; 2, 37-37.4°C; 3, <37°C. To assess neurological status, each ferret was individually placed in a
542 single-ventilated cage at the time of evaluation to observe its response to a novel environment.
543 Neurological scoring was partially adapted from the Merck Veterinary Manual (*55*) and assigned as
544 follows: 0, explores objects, weasel war dance(*56*), intact reflexes (pinch test); 1, decreased interest in
545 exploring objects; 2, lethargic, and/or altered gait, and/or decreased reflexes; 3, obtunded, and/or
546 seizures, and/or paralysis in one or more limbs. Upon reaching the predetermined endpoint, a clinical
547 score of 3 in either category, ferrets were euthanized.

548 **Multidose tolerability studies in cotton rats and ferrets**

549 Cotton rats: Female cotton rats (Envigo), aged 2-3 months were habituated for at least three days
550 prior to the beginning of the study. Cotton rats were weighed and administered GHP-88310 twice daily
551 by oral gavage at doses of 300, 600 and 1,200 mg/kg. The compound was formulated in 0.5%
552 methylcellulose, 5 mM sodium citrate, and 0.25% Tween80, with a final gavage volume of 500 µl. Each
553 animal received a total of 14 doses and was monitored daily for bodyweight and temperature using
554 implantable electronic ID transponders (TP-1000, BMDS). Following the final dose, blood samples (150
555 µl) were collected at designated time points, centrifuged at 2,000 rpm for 5 minutes at 4°C, and the
556 plasma was stored at -80°C.

557 Ferrets: Female ferrets (Triple F Farm), between 6-8 months old, were allowed to rest for at least
558 three days. Ferrets were weighed and dosed with GHP-88309 or GHP-88310 twice daily via oral
559 gavage at doses ranging from 50-1,000 mg/kg. The compounds were formulated in 1% methylcellulose,

560 with a final gavage volume of 2 ml. Animals were weighed daily, and body temperature was measured
561 using a rectal probe. Ferrets received a total of 14 doses under a twice-daily dosing regimen or 7 doses
562 under a once-daily regimen. Blood samples were collected on days 0, 2, 4, 5, 6 and 7 post-dosing for
563 complete blood cell (CBC) analysis, and on days 1 or 2 and 7 for blood chemistry analysis. CBC
564 analysis was performed using a Vetscan HM5 hematology analyzer (Abaxis), following the
565 manufacturer's protocol. For the 500 mg/kg and 1,000 mg/kg dosing groups, as well as the multi-dose
566 once-daily dosing study, maximum plasma concentration (C_{max}) at 5 hours post-dose was measured
567 after doses 1, 2, 4, 6, 8, 10, 12, and 14, or daily (once-daily regimen only). Blood samples (150 µl) were
568 collected for plasma preparation as previously described.

569 ***In vivo* infections with SeV, HPIV3 and CDV**

570 Efficacy studies in mice: Female 129x1/SvJ mice (The Jackson Laboratory), 6 weeks of age, were
571 acclimated for at least three days before being randomly assigned to study groups and housed under
572 ABSL-2 conditions for infections with sequence-validated rSeV. Bodyweight and rectal temperature
573 were measured once daily. For infection, mice were anesthetized with isoflurane and intranasally
574 inoculated with 5×10^6 $TCID_{50}$ units/ml of rSeV (*23*) in a total volume of 50 µl PBS (25 µl per nare).
575 Treatment was initiated 24 hours post-infection and administered twice-daily via oral gavage at a dose
576 of 150 mg/kg in 200 µl of 1% methylcellulose, continuing through study day 8. A subset of animals was
577 euthanized either five days post-infection or upon reaching a predetermined endpoint, and tracheas
578 and lungs were collected for analysis.

579 Efficacy studies in cotton rats: Female cotton rats (Envigo), 3-4 weeks of age, were allowed to rest
580 for at least three days prior to being randomly assigned to study groups and single-housed under
581 ABSL-2 conditions for infections with sequence-validated HPIV3 clinical isolate 13J5. Bodyweight and
582 body temperature, using an implanted electronic ID transponder (TP-1000, BMDS), were measured
583 once daily. For infection, cotton rats were anesthetized with isoflurane and intranasally inoculated with
584 1×10^7 pfu/ml of HPIV3 in a total volume of 100 µl PBS (50 µl per nare). For therapeutic dosing, animals
585 were anesthetized with isoflurane 12 hours post-infection and administered GHP-88309 or GHP-88310
586 in 500 µl of 1% methylcellulose via oral gavage, either once or twice-daily, through study day 3.

587 Efficacy studies in ferrets: CDV unvaccinated female ferrets (Triple F Farms), 8 months of age,
588 were rested for one week prior to random assignment into study groups and housed in groups of three
589 animals under ABSL-2 condition. Bodyweight and rectal temperature were recorded once daily. Ferrets
590 were anesthetized with dexmedetomidine/ketamine and intranasally inoculated with 2×10^5 $TCID_{50}$ units
591 of CDV 5804p in a total volume of 200 µl PBS (100 µl per nare) (*25*). Daily, nasal lavages were
592 performed using 1 ml of PBS supplemented with 2× antibiotics-antimycotics (Gibco). Peripheral blood
593 mononuclear cells (PBMCs) were collected twice weekly for titration of cell-associated viremia and CBC
594 analysis. On days 17, 21, and 35 post-infection blood samples were collected to assess neutralizing
595 antibody titers. For therapeutic treatments, ferrets were administered GHP-88310 by oral gavage
596 following either a once or twice-daily regimen (50-300 mg/kg) in 2 ml of 1% methylcellulose, beginning
597 at 3-days post-infection. Ferrets were euthanized either upon reaching a predetermined study endpoint
598 or at the conclusion of the study on day 35 post-infection.

599 **Virus titration of tissue samples (mice and cotton rats) and nasal lavages (ferrets only)**

600 Organs were weighed and homogenized in 300 µl PBS using a Bead Blaster 24R (Benchmark) set
601 to three 30 second cycles at 4°C, with one minute rest intervals between cycles. Homogenates and
602 ferret lavage samples were clarified by centrifugation at 13,000 × g for 10 minutes at 4°C, then
603 subsequently titrated. Viral titers were expressed as $TCID_{50}$ units/plaques per gram input tissue or per
604 ml.

605 **Virus titration of PBMCs (ferrets only)**

606 Blood samples were collected at specified time points twice per week. As previously described
607 (*25*), viremia was assessed by isolating PBMCs from 1 ml of whole blood. Red blood cells were lysed
608 using ACK buffer (150 mM NH_4Cl, 10 mM $KHCO_3$, 10 µM EDTA pH 7.4) for 7 minutes, followed by two
609 PBS washes and resuspension in DMEM. PBMC titers were determined by co-culturing serial dilutions
610 of purified PBMCs with VDS cells and expressed as $TCID_{50}$ per 10^6 PBMCs.

611 **Neutralizing antibody assay (ferrets only)**

612 Blood samples (300 µl) were collected on days 17 and 21 post-CDV infection (and on day 35 for
613 the ferret CDV QD study only) to obtain plasma, which was subjected to heat inactivation (56°C, 30

614 minutes) and clearance centrifugation (4,000 × g, 5 minutes). Heat-inactivated and clarified plasma was
615 diluted two-fold in serum free DMEM, with a final volume of 50 µl per well. Fifty microliters of rCDV
616 5804p (2×10^3 $TCID_{50}$ units) was added to the plasma dilutions, followed by incubation of the plasma-
617 virus mixture at 37°C for 75 minutes. Subsequently, the mixture was added in duplicate to VDS cells in
618 96-well plates, incubated for 3 days, and cytopathic effect was assessed by light microscopy.

619 **Whole genome sequencing of virus stocks and ferret nasal lavage samples**

620 Whole genome sequencing (WGS) was performed using metagenomic next-generation
621 sequencing (mNGS) as described previously (*57*). Briefly, extracted RNA was treated with a TURBO
622 DNA-free Kit (Thermo Fisher, product #AM1907) to remove DNA. RNA was then reverse transcribed
623 using random hexamers (Thermo Fisher, product #N8080127) and Superscript IV (Thermo Fisher,
624 product #18090010), following the manufacturer's protocol. Double-stranded cDNA synthesis was
625 performed using Sequenase v2.0 (Thermo Fisher, product #70775Z1000UN), and the resulting cDNA
626 was purified using 1.8× AMPure XP magnetic beads (Beckman Coulter, product # A63882).

627 Metagenomic viral WGS libraries were created from purified double-stranded cDNA with
628 tagmentation reagents from the Illumina DNA Prep with Enrichment Kit (Illumina, product #20025524),
629 followed by 14 cycles of dual-indexed PCR for SeV and 18 cycles for HPIV3 and CDV isolates.
630 Amplified libraries were cleaned with 0.8× AMPure XP magnetic beads. Viral isolate libraries were not
631 subjected to enrichment and proceeded directly to sequencing. Libraries were sequenced 2×150 bp on
632 NextSeq 2000 (CDV, HPIV3) or NovaSeq 6000 (SeV).

633 Due to its high viral titer, the sample "CDV ferret study - BID treatment – 50 mg/kg - ferret 2 – D8pI"
634 was sequenced using metagenomic WGS on NextSeq 2000 with 1×100 bp read format.

635 Viral WGS was also performed on all ferret nasal lavage samples with detectable PFU titers,
636 except "CDV ferret study - BID treatment – 50 mg/kg - ferret 2 – D8pI". These samples were processed
637 using QIAseq xHYB Microbial Hyb&Lib Kit A (Qiagen, product #334525) and a custom Qiagen
638 hybridization panel containing probes designed from CDV strain 5804 (AY386315.1) containing eGFP
639 reporter (Qiagen, product # 334586). Following the manufacturer's protocol, extracted RNA was
640 depleted of ribosomal RNA and converted to double-stranded cDNA. Double-stranded cDNA was then

641 enzymatically fragmented, end-repaired, indexed, purified with 0.9× and 1.1× bead cleanup, and
642 amplified with 14 cycles of PCR, followed by a final bead purification, according to the manufacturer's
643 protocol.

644 Pre-capture sequencing libraries were pooled based on PFU titer, with one to four samples per
645 pool, and incubated with the custom capture panel. After overnight hybridization with biotinylated
646 probes, probe-target hybrids were bound to streptavidin-coated magnetic beads and washed to remove
647 unbound library fragments. The enriched libraries were amplified with 20 cycles of post-hybridization
648 PCR and purified via 1.1× bead clean-up. Post-amplification library fragment sizes were estimated with
649 the TapeStation 4200 D1000 (Agilent), and concentrations were measured with Qubit 4 Fluorometer
650 and Qubit dsDNA HS Assay Kit. Libraries were sequenced on Illumina NextSeq 2000 instruments using
651 a 1×100 bp read format.

652 Data analysis: Raw reads were trimmed and quality filtered using fastp (v0.23.4)(*58*) with the
653 following parameters: --cut_mean_quality 20 --cut_front --cut_tail --length_required 20 --
654 low_complexity_filter --trim_poly_g --trim_poly_x. The consensus sequence of "recCDV_5804p WT"
655 was generated by majority voting with Geneious Prime 2025.0, using the CDV plasmid sequence
656 (AY386315.1 background) containing eGFP reporter as a reference.

657 Variants were identified using RAVA workflow with default parameters
658 (https://github.com/greninger-lab/RAVA_Pipeline/tree/publication_GSU_2025_03_01)(*59*), (*60*) .
659 References used in RAVA analysis: for "recCDV_5804p WT" we used plasmid map as a reference
660 (AY386315.1 background), for the "HPIV3 clinical isolate 13J5" – HPIV3/Seattle/USA/13J5/2016
661 (KY629774.1), for "recSeV_GFP" – Respirovirus muris strain 52 (MH557085.1), and, finally, for CDV
662 ferret nasal lavage samples – "recCDV_5804p WT" consensus sequence. Sample "CDV ferret study -
663 BID treatment – 50 mg/kg - ferret 2 – D8pI" had insufficient coverage (mean coverage of ~49x with
664 some CDS regions having 0x coverage) and was therefore excluded from the RAVA analysis.
665 Complete lists of identified non-synonymous and complex SNVs (allelic frequency ≥ 5%, sequencing
666 depth of the nucleotide position ≥ 30) can be found in the supplementary data file S1. Data availability:
667 raw sequencing data is publicly available in NCBI BioProject PRJNA1217449.

668 ***In silico* docking**

669 Docking studies were performed with MOE (version 2024.06). A structure of MeV L (Protein Data
670 Bank (PDB) 9dus) was used for the docking studies. After protonation and energy minimization, the
671 triangle matcher method was used for initial compound placement, followed by refinement using an
672 induced-fit protocol to dock GHP-88310 or GHP-88309 in the L structure based on resistance data
673 information. For MeV L, residues Y942, A866, and I1009 were selected to identify the target site for
674 docking and resulting docking poses from each polymerase target were compared. The top scoring
675 docking poses conserved between GHP-88309 and GHP-88310 were chosen for further analysis.

676 **Cellular uptake and clearance in undifferentiated NHBE cells**

677 Primary normal HBTECs (donor "F3") were seeded in 48 well plates and utilized for a wash-
678 in/wash-out study once confluency was achieved.

679 Wash-in study: An 80 μM dilution of GHP-88310 was prepared in pre-warmed Lifeline media.
680 Following media removal from the cells, 0.5 ml of either the 80 μM compound or vehicle (volume
681 equivalent DMSO)-media mixture was added to the wells. Plates were incubated at 37°C, 5% CO_2 and
682 extracted in triplicate at the indicated time points. Cells were washed twice with cold DPBS, followed by
683 the addition of 250 μl of 70% methanol/30% water spiked with the internal standard to each well treated
684 with GHP-88310. A mock-treated blank plate (16 well) was extracted with 250 μl of 70% methanol/30%
685 water (no internal standard) per well at one-hour post-dosing. All samples were mixed by pipetting and
686 transferred to 1.5 ml microcentrifuge tubes. After centrifugation at 16,000 × g for 10 minutes at 4°C, the
687 supernatants were transferred to 2 ml tubes and stored at -80°C until LC/MS/MS analysis.

688 Wash-out study: An 80 μM dilution of GHP-88310 was prepared in pre-warmed lifeline media. After
689 media removal, 0.5 ml of the 80 μM compound-media mixture was added to the wells. Plates were
690 incubated at 37°C, 5% CO_2 for one hour, washed twice with 0.5 ml warm DPBS, and compound free
691 pre-warmed Lifeline media was added. Plates were further incubated as specified, followed by washing
692 (twice with 0.5 ml cold DPBS) and extraction, processing, and analysis as described above.

693 **Recapitulation of ferret plasma PK profile in EpiAirways**

694 Air liquid interface HAE cells were exposed basolaterally to dynamic GHP-88310 concentrations
695 reflected ferret plasma levels after either 50 mg/kg oral twice-daily dosing on day 7 or a single oral dose
696 of 20 mg/kg. All ALI HAE cell cultures (n=4 per condition: vehicle, 50 or 20 mg/kg bid, and 50 or 20
697 mg/kg qd) were infected with 1×10^4 PFU per well of the HPIV3 clinical isolate 13J5 one hour prior to
698 treatment. Infected cultures underwent either four 12-hour treatment cycles (bid) or two 24-hour
699 treatment cycles (qd). Twenty hours post infection the apical side was rinsed once with 400 µl PBS to
700 reduce mucus accumulation. After 48 hours post-infection, apically shed virus was collected by
701 incubating the cultures with 300 µl of DPBS at 37°C for 30 minutes. Viral titers were then determined by
702 plaque assay on Vero E6 TMPRSS2 cells.

703 **Statistical analysis and data preparation**

704 For statistical analysis of studies comparing more than two study groups, a one-way analysis of
705 variance (ANOVA) or two-way ANOVA with multiple comparison *post hoc* tests as specified were used
706 to assess statistical difference between samples. An unpaired, two-tailed t-test was used to compare
707 compound concentrations across the analyzed organs. Statistical analyses were performed using
708 GraphPad Prism (v10.1.0). All figures were assembled in GraphPad Prism and Adobe
709 Illustrator/Photoshop. Study schematics were created using Adobe Illustrator, with animal illustrations
710 generated via the vector tool. Objects in figures 5 and 6 were drawn in Adobe Illustrator and adapted
711 from BioRender. The number of individual biological replicates (n values) and exact P values are shown
712 in the figures. The threshold of statistical significance (α) was set to 0.05. Source data and statistical
713 analysis are shown in the source data (supplementary data file 2) and statistical analysis
714 (supplementary data file 3) files, respectively.

715 **Ethical compliance**

716 All animal work was performed in compliance with the *Guide for the Care and Use of Laboratory*
717 *Animals* of the National Institutes of Health and the Animal Welfare Act Code of Federal Regulations.
718 Experiments involving mice, cotton rats and ferrets were approved by the Georgia State University
719 Institutional Animal Care and Use Committee (IACUC) under protocols A23011, A24022 and A22035,
720 respectively. All experiments using infectious material were approved by the Georgia State University

721 Institutional Biosafety Committee (IBCs) and performed in BSL-2/ABSL-2 containment facilities,
722 respectively.

723 **Materials & Correspondence**

724 Correspondence and material requests should be addressed to R.K. Plemper, rplemper@gsu.edu

725

726 **List of Supplementary Materials**

727 Table S1. Elemental analysis of selected GHP-88309 analogs

728 Figure S1. Multi-dose tolerability of GHP-88309 in ferrets

729 Figure S2. Clinical parameters of SeV infection in mice

730 Figure S3. Clinical parameters and viral titers of cotton rats infected with HPIV3

731 Figure S4. Multi-dose tolerability in cotton rats

732 Figure S5. Once daily administration of GHP-88310 against HPIV3 in cotton rats

733 Figure S6. Multi-dose tolerability and CBC parameters in ferrets

734 Figure S7. Clinical parameters of multi-dose GHP-88309 and GHP-88310 tolerability

735 Figure S8. Evaluation of once- and twice-daily GHP-88310 dosing for CDV infection in ferrets

736 Figure S9. *In silico* docking of GHP-88309

737 Figure S10. 2D docking poses

738 Figure S11. Cellular uptake and retention of GHP-88310

739 Figure S12. Confocal imaging of GHP-88310 antiviral activity in human airway epithelium organoids

740

741 **References and Notes**

742 1. R. K. Plemper, R. A. Lamb, in *Fields Virology,* D. M. Knipe, P. M. Howley, S. Whelan, Eds.
743 (Wolters Kluwer/Lippincott Williams & Wilkins, Philadelphia, 2020), vol. 1, chap. 33, pp. 504-558.
744 2. B. Lee, C. C. Broder, L. Wang, in *Fields Virology,* D. M. Knipe, P. M. Howley, S. Whelan, Eds.
745 (Wolters Kluwer/Lippincott Williams & Wilkins, Philadelphia, 2200), vol. 1, chap. 34, pp. 559-595.
746 3. A. J. Wakefield *et al.*, RETRACTED: Ileal-lymphoid-nodular hyperplasia, non-specific colitis, and
747 pervasive developmental disorder in children. *The Lancet* **351**, 637-641 (1998).
748 4. L. Eggertson, Lancet retracts 12-year-old article linking autism to MMR vaccines. *Cmaj* **182**,
749 E199-200 (2010).
750 5. H. J. Larson, E. Gakidou, C. J. L. Murray, The Vaccine-Hesitant Moment. *N Engl J Med* **387**, 58-
751 65 (2022).
752 6. L. A. H. Do, K. Mulholland, Measles 2025. *N Engl J Med*, (2025).
753 7. CDC. (2025), vol. 2025.
754 8. W. H. Organization, in *Disease Outbreak News*. (2025), vol. 2025.

9. G. o. Canada, in *Weekly surveillance reports and monitoring maps for measles and rubella.* (2025), vol. 2025.
10. NMA Statement on Measles Outbreak – Children's Lives in Danger in West Texas. https://nmanet.org/press-release/nma-statement-on-measles-outbreak-childrens-lives-in-danger-in-west-texas/ (accessed 02/27/2025). (2025).
11. R. K. Plemper, Measles Resurgence and Drug Development. *Curr. Opin. Virol.* **41**, 8-17 (2020).
12. D. V. Parums, A Review of the Resurgence of Measles, a Vaccine-Preventable Disease, as Current Concerns Contrast with Past Hopes for Measles Elimination. *Med Sci Monit* **30**, e944436 (2024).
13. S. S. Chen. (emedicine.medscape, 2025), vol. 2025.
14. S. E. Kern, Challenges in conducting clinical trials in children: approaches for improving performance. *Expert Rev Clin Pharmacol* **2**, 609-617 (2009).
15. V. Bencheva, N. K. Mann, T. Rombey, D. Pieper, S. Schmiedl, Barriers and facilitators to enrollment in pediatric clinical trials: an overview of systematic reviews. *Syst Rev* **13**, 283 (2024).
16. C. Domingues, I. Jarak, F. Veiga, M. Dourado, A. Figueiras, Pediatric Drug Development: Reviewing Challenges and Opportunities by Tracking Innovative Therapies. *Pharmaceutics*. 2023 (10.3390/pharmaceutics15102431).
17. R. H. Parrott *et al.*, Clinical features of infection with hemadsorption viruses. *N. Engl. J. Med.* **260**, 731-738 (1959).
18. R. C. Welliver, D. T. Wong, M. Sun, N. McCarthy, Parainfluenza virus bronchiolitis. Epidemiology and pathogenesis. *Am. J. Dis. Child.* **140**, 34-40 (1986).
19. A. J. Peck *et al.*, Respiratory virus infection among hematopoietic cell transplant recipients: evidence for asymptomatic parainfluenza virus infection. *Blood* **110**, 1681-1688 (2007).
20. W. G. Nichols, L. Corey, T. Gooley, C. Davis, M. Boeckh, Parainfluenza virus infections after hematopoietic stem cell transplantation: risk factors, response to antiviral therapy, and effect on transplant outcome. *Blood* **98**, 573-578 (2001).
21. M. S. Lee, R. E. Walker, P. M. Mendelman, Medical burden of respiratory syncytial virus and parainfluenza virus type 3 infection among US children. Implications for design of vaccine trials. *Hum Vaccin* **1**, 6-11 (2005).
22. G. R. Abedi *et al.*, Estimates of Parainfluenza Virus-Associated Hospitalizations and Cost Among Children Aged Less Than 5 Years in the United States, 1998-2010. *J Pediatric Infect Dis Soc* **5**, 7-13 (2016).
23. R. M. Cox *et al.*, Orally efficacious broad-spectrum allosteric inhibitor of paramyxovirus polymerase. *Nat Microbiol* **5**, 1232-1246 (2020).
24. G. D. Haas *et al.*, Tetracistronic Minigenomes Elucidate a Functional Promoter for Ghana Virus and Unveils Cedar Virus Replicase Promiscuity for all Henipaviruses. *bioRxiv*, (2024).
25. R. M. Cox *et al.*, Therapeutic mitigation of measles-like immune amnesia and exacerbated disease after prior respiratory virus infections in ferrets. *Nat Commun* **15**, 1189 (2024).
26. J. D. Wolf, M. R. Sirrine, R. M. Cox, R. K. Plemper, Structural basis of paramyxo- and pneumovirus polymerase inhibition by non-nucleoside small-molecule antivirals. *Antimicrob Agents Chemother* **68**, e0080024 (2024).
27. P. A. Rota *et al.*, Measles. *Nature Reviews Disease Primers* **2**, 16049 (2016).
28. A. T. Truong *et al.*, Genetic analysis of Asian measles virus strains – new endemic genotype in Nepal. *Virus Research* **76**, 71-78 (2001).
29. Y. Wang *et al.*, Structures of the measles virus polymerase complex with non-nucleoside inhibitors and mechanism of inhibition. *Cell* **188**, 4913-4923.e4913 (2025).
30. D. Wang, G. Yang, B. Liu, Structure of the measles virus ternary polymerase complex. *Nature Communications* **16**, 3819 (2025).
31. B. Srinivasan *et al.*, TEER measurement techniques for in vitro barrier model systems. *J Lab Autom* **20**, 107-126 (2015).
32. M. Malik, S. A. Steele, D. Mitra, C. J. Long, J. J. Hickman, Trans-epithelial/endothelial electrical resistance (TEER): Current state of integrated TEER measurements in organ-on-a-chip devices. *Current Opinion in Biomedical Engineering* **34**, 100588 (2025).

33. A. R. Calabro, R. Konsoula, F. A. Barile, Evaluation of in vitro cytotoxicity and paracellular permeability of intact monolayers with mouse embryonic stem cells. *Toxicology in Vitro* **22**, 1273-1284 (2008).
34. L. C. Rijsbergen *et al.*, Modeling Infection and Tropism of Human Parainfluenza Virus Type 3 in Ferrets. *mBio* **13**, e0383121 (2021).
35. L. Zhang *et al.*, Infection of ciliated cells by human parainfluenza virus type 3 in an in vitro model of human airway epithelium. *J Virol* **79**, 1113-1124 (2005).
36. B. Martin, S. Ji, S. Maudsley, M. P. Mattson, "Control" laboratory rodents are metabolically morbid: why it matters. *Proc Natl Acad Sci U S A* **107**, 6127-6133 (2010).
37. C. Moro, C. Magnan, Revisited guidelines for metabolic tolerance tests in mice. *Lab Animal* **54**, 16-23 (2025).
38. J. K. Corrigan *et al.*, A big-data approach to understanding metabolic rate and response to obesity in laboratory mice. *eLife* **9**, e53560 (2020).
39. M. Martignoni, G. M. Groothuis, R. de Kanter, Species differences between mouse, rat, dog, monkey and human CYP-mediated drug metabolism, inhibition and induction. *Expert Opin Drug Metab Toxicol* **2**, 875-894 (2006).
40. T. Nakajima *et al.*, Cytochrome P450-related differences between rats and mice in the metabolism of benzene, toluene and trichloroethylene in liver microsomes. *Biochem Pharmacol* **45**, 1079-1085 (1993).
41. U. M. Zanger, M. Schwab, Cytochrome P450 enzymes in drug metabolism: Regulation of gene expression, enzyme activities, and impact of genetic variation. *Pharmacology & Therapeutics* **138**, 103-141 (2013).
42. R. Mezencev *et al.*, The association between histopathologic effects and liver weight changes induced in mice and rats by chemical exposures: an analysis of the data from Toxicity Reference Database (ToxRefDB). *Toxicol Sci* **200**, 404-413 (2024).
43. S. P. Jiang *et al.*, Airway Organoid Models as Pivotal Tools for Unraveling Molecular Mechanisms and Therapeutic Targets in Respiratory Diseases: A Literature Review. *Ther Clin Risk Manag* **21**, 975-986 (2025).
44. H. Joo, S. Min, S. W. Cho, Advanced lung organoids for respiratory system and pulmonary disease modeling. *J Tissue Eng* **15**, 20417314241232502 (2024).
45. J. H. Lee *et al.*, Development of robust antiviral assays using relevant apical-out human airway organoids. *bioRxiv*, (2024).
46. C. T. Ekanger *et al.*, Comparison of air-liquid interface transwell and airway organoid models for human respiratory virus infection studies. *Front Immunol* **16**, 1532144 (2025).
47. M. Toots *et al.*, Characterization of orally efficacious influenza drug with high resistance barrier in ferrets and human airway epithelia. *Sci. Transl. Med.* **11**, (2019).
48. A. Nair, M. A. Morsy, S. Jacob, Dose translation between laboratory animals and human in preclinical and clinical phases of drug development. *Drug Dev Res* **79**, 373-382 (2018).
49. S. Plumet, W. P. Duprex, D. Gerlier, Dynamics of viral RNA synthesis during measles virus infection. *J. Virol.* **79**, 6900-6908 (2005).
50. T. Komatsu, K. Takeuchi, J. Yokoo, B. Gotoh, C and V proteins of Sendai virus target signaling pathways leading to IRF-3 activation for the negative regulation of interferon-β production. *Virology* **325**, 137-148 (2004).
51. A. Kato *et al.*, Y2, the smallest of the Sendai virus C proteins, is fully capable of both counteracting the antiviral action of interferons and inhibiting viral RNA synthesis. *J Virol* **75**, 3802-3810 (2001).
52. B. Gotoh *et al.*, Knockout of the Sendai virus C gene eliminates the viral ability to prevent the interferon-alpha/beta-mediated responses. *FEBS Lett* **459**, 205-210 (1999).
53. D. Garcin, P. Latorre, D. Kolakofsky, Sendai virus C proteins counteract the interferon-mediated induction of an antiviral state. *J Virol* **73**, 6559-6565 (1999).
54. J. Sourimant *et al.*, 4'-Fluorouridine is an oral antiviral that blocks respiratory syncytial virus and SARS-CoV-2 replication. *Science* **375**, 161-167 (2022).
55. W. B. Thomas. (2023), vol. 2025.
56. M. J. Goodfellow *et al.*, Behavioral assessment of well-being in the naïve laboratory ferret (Mustela putorius furo). *Sci Rep* **14**, 30119 (2024).

862 57. A. L. Greninger *et al.*, Rapid Metagenomic Next-Generation Sequencing during an Investigation
863 of Hospital-Acquired Human Parainfluenza Virus 3 Infections. *J. Clin. Microbiol.* **55**, 177-182
864 (2017).
865 58. S. Chen, Y. Zhou, Y. Chen, J. Gu, fastp: an ultra-fast all-in-one FASTQ preprocessor.
866 *Bioinformatics* **34**, i884-i890 (2018).
867 59. P. Di Tommaso *et al.*, Nextflow enables reproducible computational workflows. *Nat Biotechnol*
868 **35**, 316-319 (2017).
869 60. M. J. Lin, R. C. Shean, N. Makhsous, A. L. Greninger, LAVA: a streamlined visualization tool for
870 longitudinal analysis of viral alleles. *bioRxiv*, 2019.2012.2017.879320 (2019).
871

872 **Acknowledgements**

873 We thank the Georgia State University Department of Animal Resources for expert assistance and
874 M. Sirrine for assistance. The recHPIV3 and recCDV-5804p genomic plasmids and Vero-canine SLAM
875 cells were kind gifts of B. Lee, V. von Messling, and Y. Yanagi, respectively. Blood chemistry analysis
876 was provided by the Pathology Core of Emory University. This study was supported, in part, by public
877 health service grants AI071002 (to R.K.P.), AI171403 project 3 (to R.K.P.), AI171403 Scientific Core B
878 (to M.G.N), AI171403 Scientific Core C, and AI171403 Scientific Core D (to A.L.G.) from the NIH/NIAID.
879

880 **Competing interests**

881 CML, MG, RMC, MGN, and RKP are co-inventors on a patent filing covering composition and method
882 of use of GHP-88310/EIDD-3608 for antiviral therapy. This study could affect their personal financial
883 status. RKP reports contract testing to GSU from Enanta Pharmaceuticals and Gilead Sciences, outside
884 of the described work. ALG reports contract testing to UW from Abbott, Cepheid, Novavax, Pfizer,
885 Janssen and Hologic, research support from Gilead, and personal fees from Arisan Therapeutics, outside
886 of the described work. All other authors declare that they have no competing interests to report.

887 **Figures**

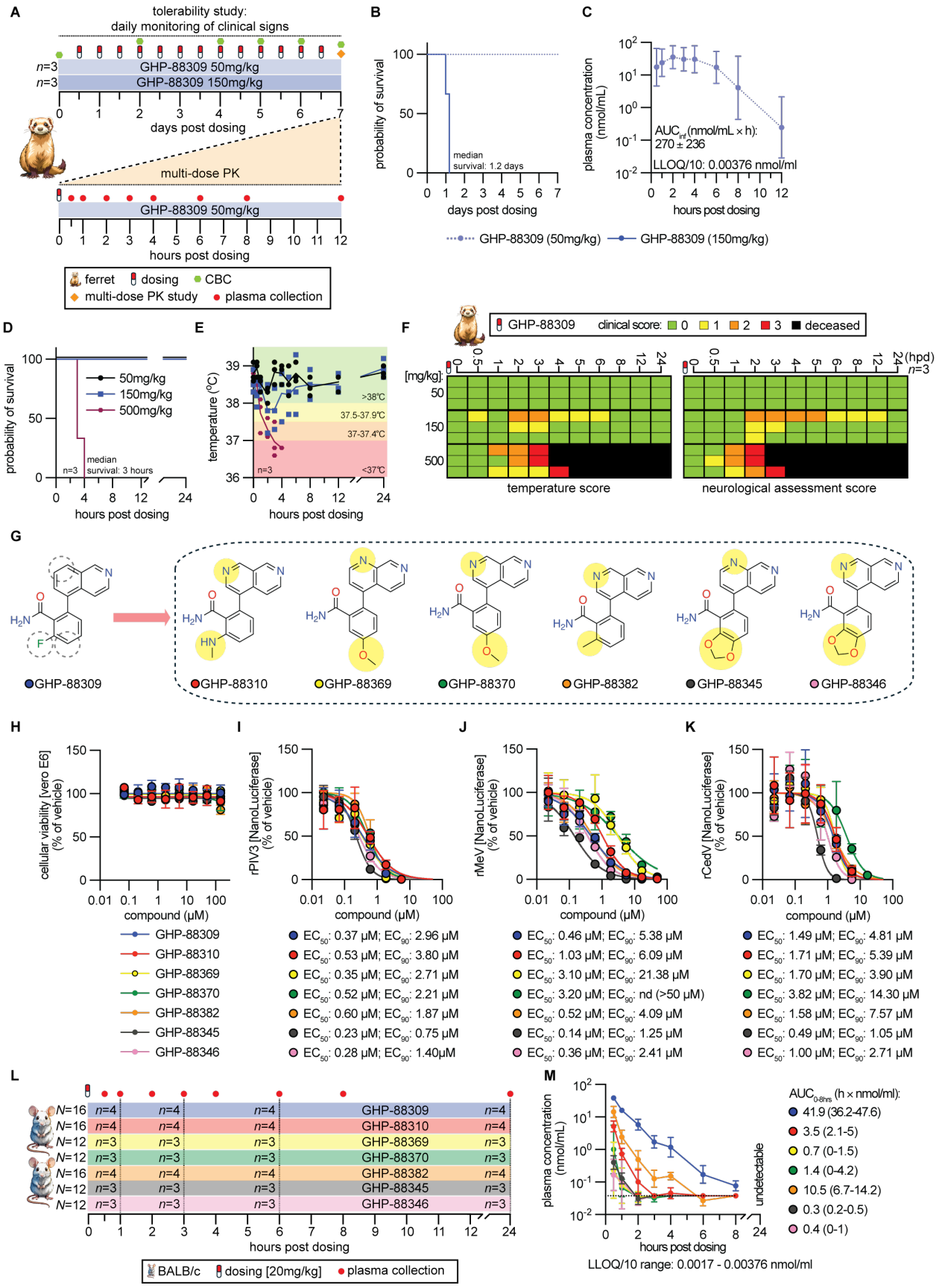

888

889 **Figure 1. SAR development of broad-spectrum GHP-class polymerase inhibitors. A)** Study
890 schematic of multi-dose GHP-88309 tolerability and PK assessment. Ferrets received 14 oral doses of
891 GHP-88309 at two different concentrations, administered twice daily. **B)** Survival curves of animals
892 from (A). **C)** PK profile of GHP-88309 (50 mg/kg) in ferret plasma following 14 oral doses administered
893 b.i.d. Exposure is specified. **D-F)** Survival curves (D), body temperature (E), and clinical scores (F) of
894 animals after single oral dose of GHP-88309. Body temperature scoring: 0, >38°C; 1, 37.5-37.9°C; 2,
895 37-37.4°C; 3, <37°C. Neurologic scoring: 0, explores objects, weasel war dance, intact reflexes; 1,
896 decreased interest in exploring objects; 2, lethargic, and/or altered gait, and/or decreased reflexes; 3,
897 obtunded, and/or seizures, and/or paralysis in one or more limbs. **G)** Top-ranking GHP-88309 analogs.
898 Dashed circles mark regions that QSAR models (*23*) have identified as most amenable to synthetic
899 elaboration. **H)** Evaluation of cellular viability of GHP compounds on Vero-E6 cells. **I-K)** Recombinant
900 virus reporter-based dose response inhibition of HPIV3 (I), MeV (J), and CedV (K), n ≥3. **L)** Study
901 schematic of single-dose PK assessment in BALB/c mice. Mice received an oral dose of GHP-class (20
902 mg/kg) and were monitored over 24 hours. Blood was collected from each sub-group of mice twice,
903 following euthanasia. **M)** Single-dose PK profile in mouse plasma. Exposure is given as $AUC_{0\text{-}8hrs}$ with
904 95% confidence intervals in parenthesis. Group sizes (n) specified in study schematics (A,L). Log-rank
905 (Mantel-Cox) test with median survival shown (B,D). Symbols represent geometric mean ± geometric
906 standard deviation (SD) (C,M). Variable slope 4-parameter non-linear regression modeling (H-K), n ≥3.
907 Symbols represent means ± SD. LLOQ, lower limit of quantitation. AUC, area under the curve.

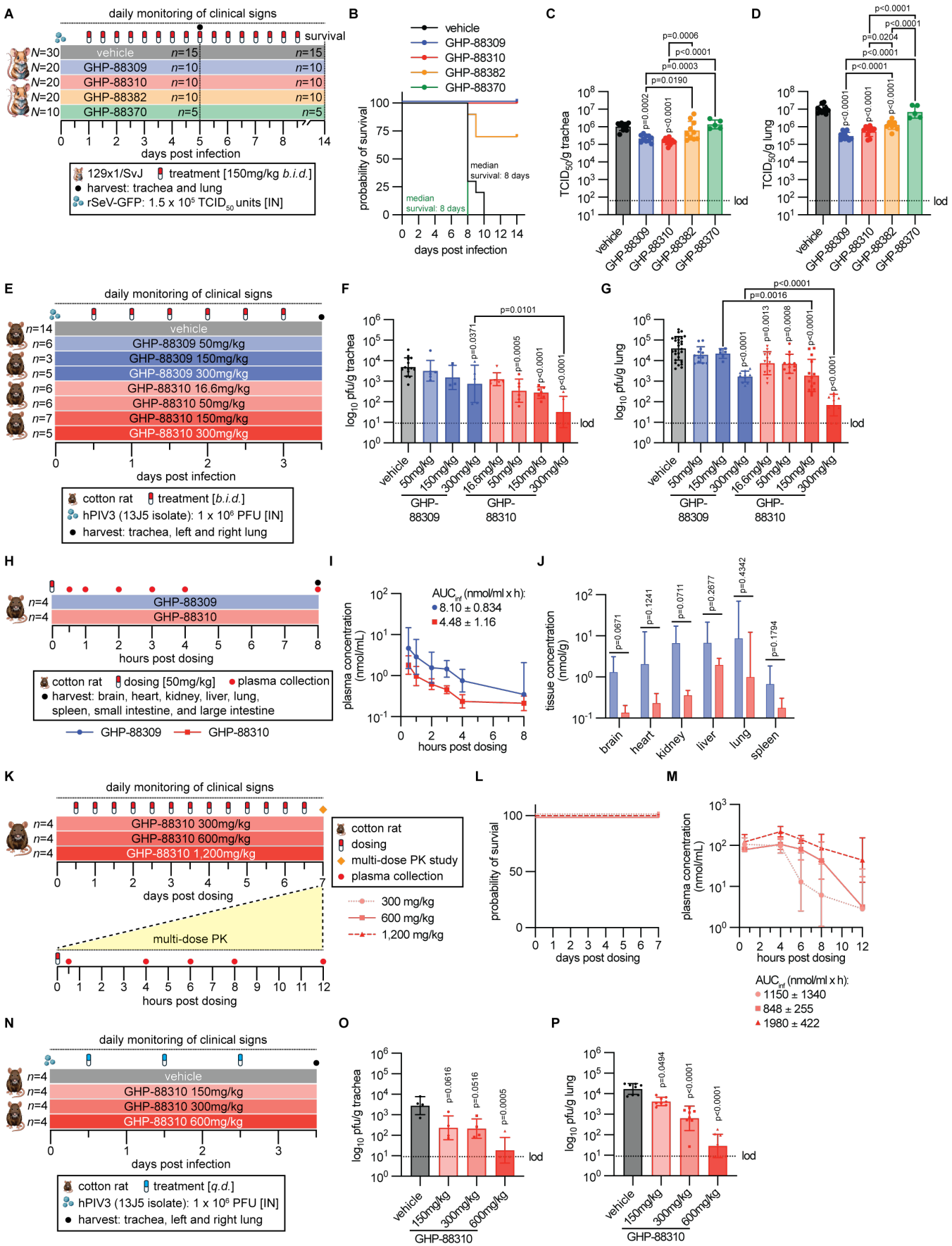
A
daily monitoring of clinical signs
survival
N=30 vehicle n=15 n=15
N=20 GHP-88309 n=10 n=10
N=20 GHP-88310 n=10 n=10
N=20 GHP-88382 n=10 n=10
N=10 GHP-88370 n=5 n=5
days post infection
129x1/SvJ
treatment [150mg/kg b.i.d.]
harvest: trachea and lung
rSeV-GFP: 1.5 x 10^5 TCID50 units [IN]
B
vehicle
GHP-88309
GHP-88310
GHP-88382
GHP-88370
probability of survival
median survival: 8 days
days post infection
C
TCID50/g trachea
lod
D
TCID50/g lung
E
daily monitoring of clinical signs
n=14 vehicle
n=6 GHP-88309 50mg/kg
n=3 GHP-88309 150mg/kg
n=5 GHP-88309 300mg/kg
n=6 GHP-88310 16.6mg/kg
n=6 GHP-88310 50mg/kg
n=7 GHP-88310 150mg/kg
n=5 GHP-88310 300mg/kg
days post infection
cotton rat
treatment [b.i.d.]
hPIV3 (13J5 isolate): 1 x 10^6 PFU [IN]
harvest: trachea, left and right lung
F
log10 pfu/g trachea
G
log10 pfu/g lung
H
n=4 GHP-88309
n=4 GHP-88310
hours post dosing
cotton rat
dosing [50mg/kg]
plasma collection
harvest: brain, heart, kidney, liver, lung, spleen, small intestine, and large intestine
I
plasma concentration (nmol/mL)
AUCinf (nmol/ml x h):
8.10 ± 0.834
4.48 ± 1.16
J
tissue concentration (nmol/g)
brain
heart
kidney
liver
lung
spleen
K
daily monitoring of clinical signs
n=4 GHP-88310 300mg/kg
n=4 GHP-88310 600mg/kg
n=4 GHP-88310 1,200mg/kg
days post dosing
multi-dose PK
hours post dosing
cotton rat
dosing
multi-dose PK study
plasma collection
300 mg/kg
600 mg/kg
1,200 mg/kg
L
probability of survival
days post dosing
M
plasma concentration (nmol/mL)
hours post dosing
AUCinf (nmol/ml x h):
1150 ± 1340
848 ± 255
1980 ± 422
N
daily monitoring of clinical signs
n=4 vehicle
n=4 GHP-88310 150mg/kg
n=4 GHP-88310 300mg/kg
n=4 GHP-88310 600mg/kg
days post infection
cotton rat
treatment [q.d.]
hPIV3 (13J5 isolate): 1 x 10^6 PFU [IN]
harvest: trachea, left and right lung
O
log10 pfu/g trachea
P
log10 pfu/g lung
GHP-88310

908

909 **Figure 2. PK and efficacy evaluation of GHP-88309 analogs in rodents. A)** Study schematic of
910 compound efficacy testing in 129x1/SvJ mice. Mice were infected intranasally with 1.5×10^5 $TCID_{50}$ units
911 of recombinant SeV. Compounds were administered orally b.i.d., starting one day after infection and
912 continuing through 8.5 dpi. **B-D)** Survival curves (B), trachea (C) and lung (D) viral titers determined 5
913 dpi of animals shown in (A). **E)** Study overview. A direct comparison of GHP-88309 and GHP-88310
914 efficacy at varying concentrations was conducted in cotton rats. Animals were intranasally infected with
915 1×10^6 $TCID_{50}$ units of HPIV3 clinical isolate 13J5. Oral dosing was initiated 12 hours post infection and
916 continued b.i.d. **F,G)** Trachea (F) and combined left and right cranial lungs (G) were collected 3.5 days
917 after infection and viral titers determined by plaque assay. **H)** Study outline of single-dose PK and tissue
918 distribution analysis in cotton rats, comparing 50 mg/kg doses of GHP-88309 and GHP-88310. **I,J)** PK
919 profiles of GHP-88309 and GHP-88310 in cotton rat plasma (I) and **t**issue concentrations of GHP-
920 88309 and GHP-88310 measured 8 hours post dosing (J). Unpaired, two-tailed t-test. Bars indicate the
921 geometric mean ± geometric SD. **K)** Overview of a multi-dose GHP-88310 tolerability and PK study.
922 Cotton rats received 14 oral doses of varying concentrations, administered twice daily. **L,M)** Survival
923 curves (L) and PK profile (M) after 14 doses of GHP-88310. **N)** Summary overview of an efficacy
924 evaluation of GHP-88310 administered once daily at different concentrations in cotton rats. Animals
925 were intranasally infected with 1×10^6 $TCID_{50}$ units of HPIV3, and oral dosing started 12 hours after
926 infection. **O,P)** Trachea (O) and combined left and right cranial lung lobes (P) were collected 3.5 dpi
927 and viral titers determined by plaque assay. In (B,L), log-rank (Mantel-Cox) test with median survival. In
928 (C,D,F,G,O,P), bars indicate the geometric mean ± geometric SD, symbols represent individual
929 biological repeats. One-way ANOVA with Tukey's (between group comparisons) or Dunnet's
930 (comparisons to vehicle) post-hoc multiple comparisons test. In (I,M), symbols represent geometric
931 means ± geometric SD.

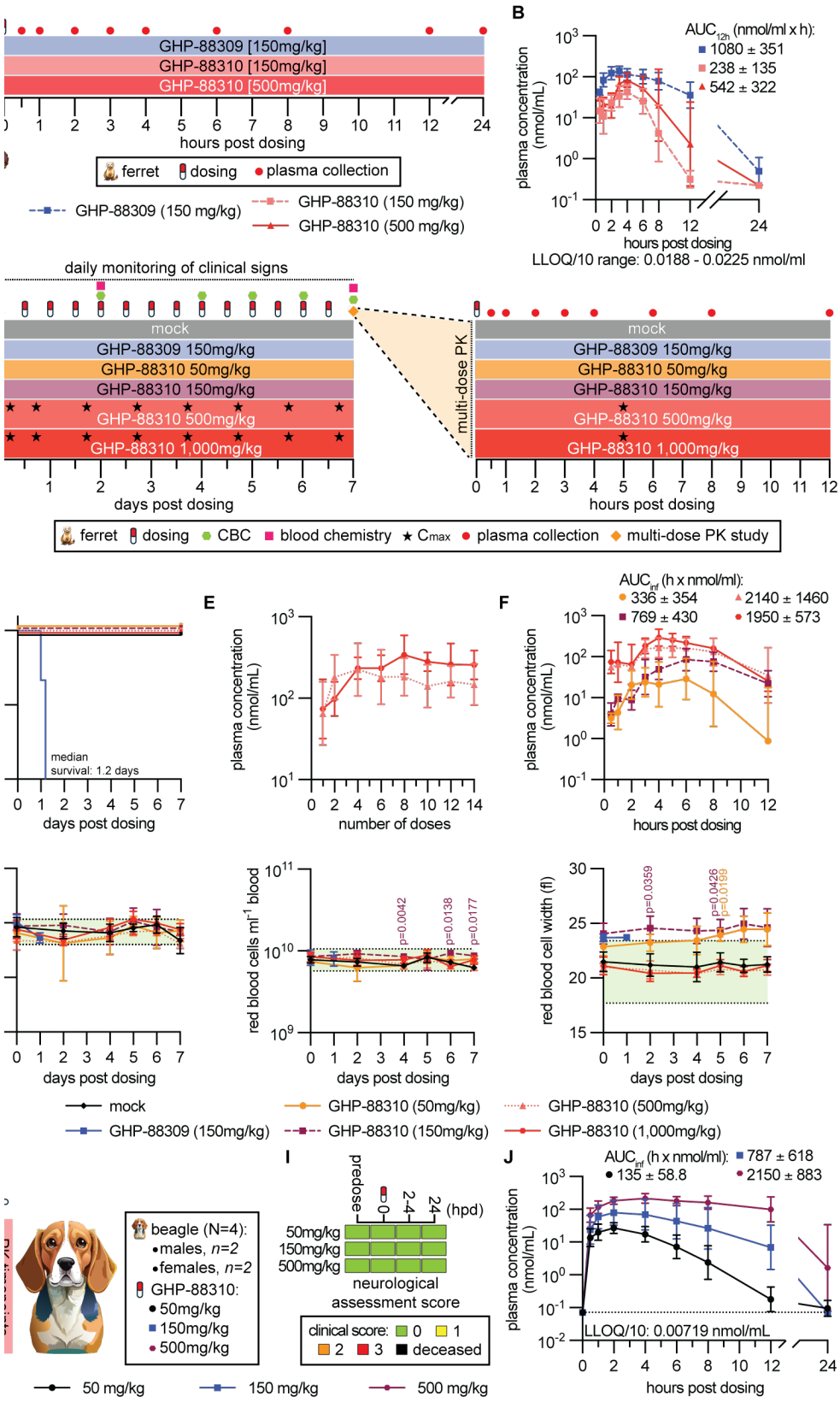

932

933 **Figure 3. Single and multi-dose tolerability and PK of twice daily GHP-88310 in ferrets. A)**

934 Overview of single oral dose PK study of GHP-88309 and GHP-88310 in ferrets. **B)** PK profile of GHP-

935 88309 and GHP-88310 in ferret plasma. **C)** Schematic of multi-dose tolerability and PK study of GHP-
936 88309 and GHP-88310 at different concentrations. Ferrets received 14 oral doses, administered b.i.d.
937 Maximal plasma concentration (C_{max}) was measured daily in ferrets administered 500 and 1,000 mg/kg
938 GHP-88310. **D)** Survival curves; data for the 150 mg/kg GHP-88309 group, originally shown in (Fig. 1A-
939 B, are included for direct comparison. Log-rank (Mantel-Cox) test with median survival. **E)** C_{max} of GHP-
940 88310 to monitor plasma build-up after doses 1, 2, 4, 6, 8, 10, 12, and 14. **F)** PK profile of GHP-88310
941 in ferret plasma after 14 oral doses. **G)** CBC analysis of ferret blood samples quantifying white blood
942 cells (left), red blood cells (middle), and red blood cell width (right). Normal range for each parameter is
943 shown in green shading. (Left, middle), symbols indicate the geometric mean ± geometric SD, (right)
944 symbols represent means ± SD. Two-way ANOVA followed by Dunnet's (comparisons to mock) post-
945 hoc multiple comparisons test. **H-J)** Single dose PK study of GHP-88310 in dogs. Shown are study
946 outline (H), neurologic status scores (I) (0, explores objects, intact reflexes; 1, decreased interest in
947 exploring objects; 2, lethargic, and/or altered gait, and/or decreased reflexes; 3, obtunded, and/or
948 seizures, and/or paralysis in one or more limbs), and PK profile of GHP-88310 in dog plasma (J). In (B,
949 E-F, J), symbols indicate geometric means ± geometric SD.

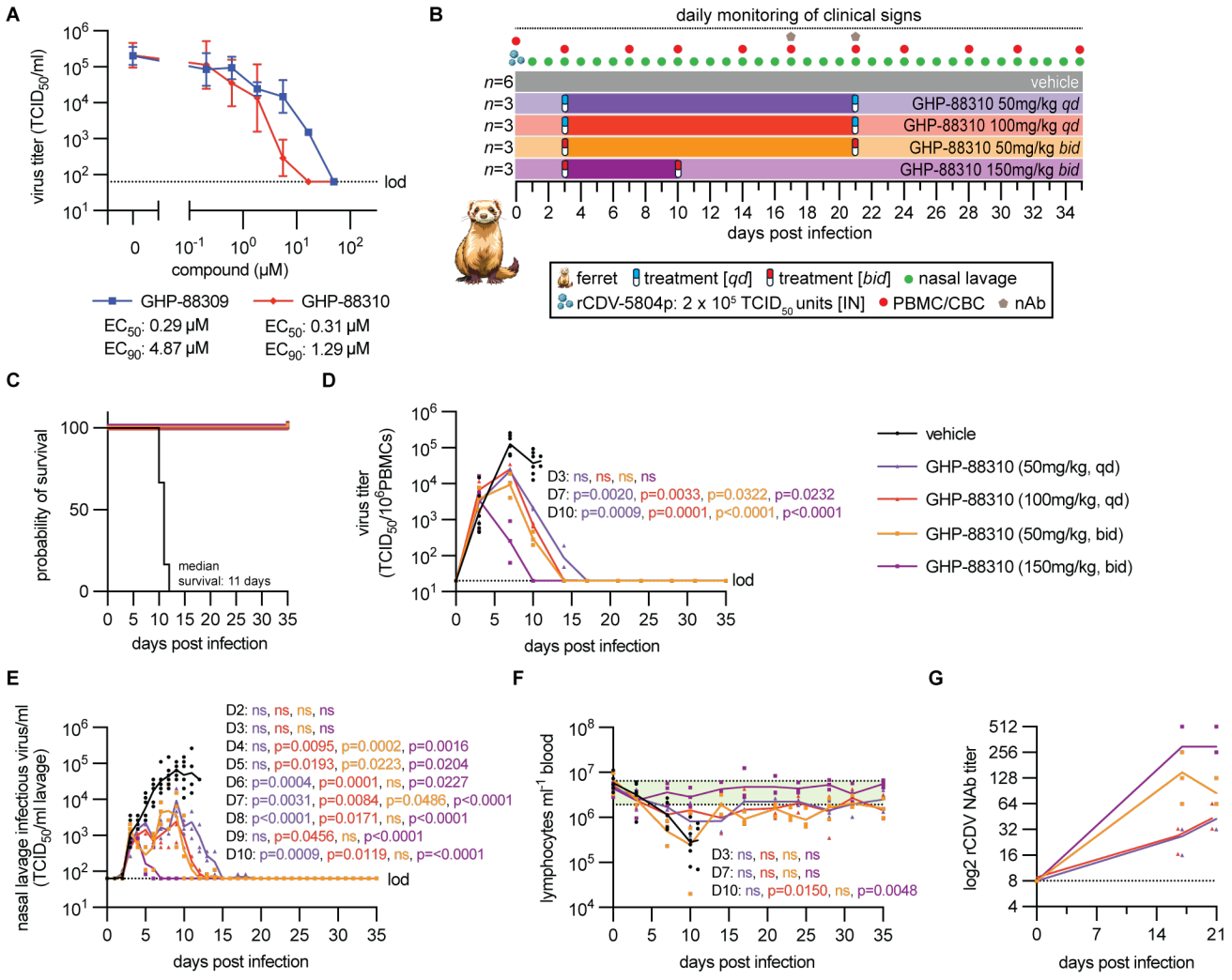

Figure 4. Therapeutic effect of GHP-88310 on CDV infection in ferrets. A) Virus yield reduction of recCDV-5804p. Variable slope 4-parameter non-linear regression modeling; n ≥3. Symbols indicate the geometric mean ± geometric SD. **B)** Overview of assessment of q.d. and b.i.d. GHP-88310 therapeutic potential. Ferrets were infected intranasally with 2×10^5 $TCID_{50}$ units of recCDV-5804p. Oral administration of GHP-88310 began 3 days after infection and continued until 10 (150 mg/kg) or 21 (50 mg/kg) dpi. **C)** Survival curves. Log-rank (Mantel-Cox) test with median survival. **D-F)** PBMC-associated viremia (D), nasal lavage viral titers quantified by $TCID_{50}$ assay (E), and lymphocyte counts (F) are shown. Normal range of lymphocytes is depicted by green shading. **G)** Neutralizing antibody titers. In (D-F), symbols indicate individual animals and lines represent geometric means. Two-way ANOVA followed by Dunnet's (comparisons to vehicle) post-hoc multiple comparisons test.

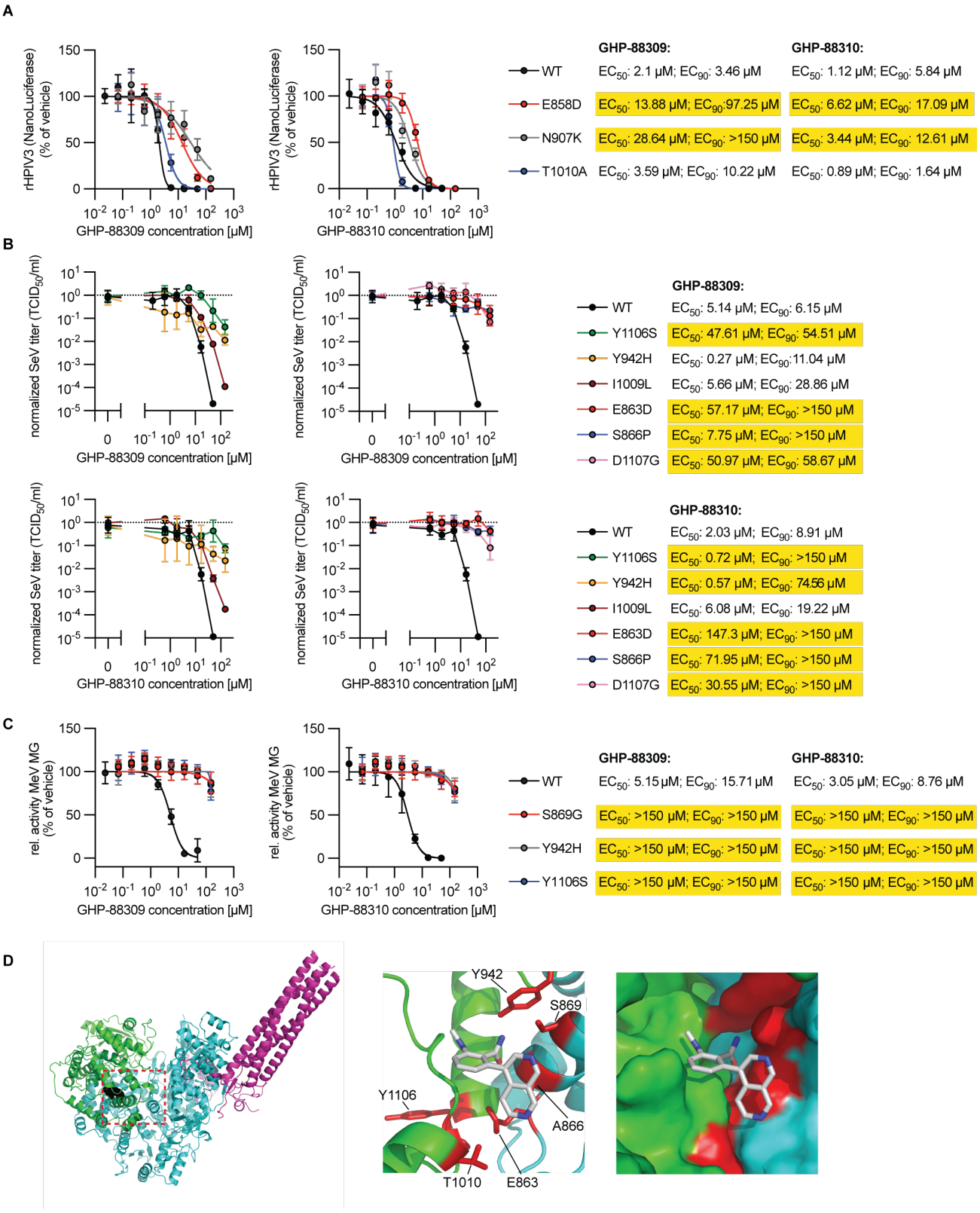

Figure 5. Functional and molecular profiling of GHP-88310. A-C) Dose-response assays with recombinant virus variants or in a minigenome harboring mutations that mediate reduced susceptibility to GHP-88309. Shown are 4-parameter variable slope non-linear regression curves for HPIV3 (A), SeV

965 (B), and in a MeV minigenome (C). Fifty and 90% inhibitory concentrations against each compound are
966 provided. Yellow highlights mark mutations that result in a ≥5-fold increase in EC_{50} and/or EC_{90}
967 compared to the unmodified genetic parent virus. **D)** *In silico* docking of GHP-88310. Ribbon
968 representation of the MeV L-P structure (PDBID: 9dus), highlighting the predicted docking location
969 (black spheres in red dashed box) of GHP-88310 (left). The RdRP and capping domains are colored in
970 cyan and green, respectively. Ribbon representation of the top scoring docking pose conserved
971 between GHP-88309 and GHP-88310 (middle). GHP-88310 docking pose is shown as grey sticks.
972 Residues that have been shown to confer resistance to GHP-88309 are highlighted in red. Surface
973 representation of the docking site of GHP-88310 showing the location of the docking pose between the
974 capping and RdRP domains (right). In (A-C), curves show 4-parameter variable slope non-linear
975 regression models; n ≥3. Symbols represent means ± SD (A,C) or the geometric mean ± geometric SD
976 (B).

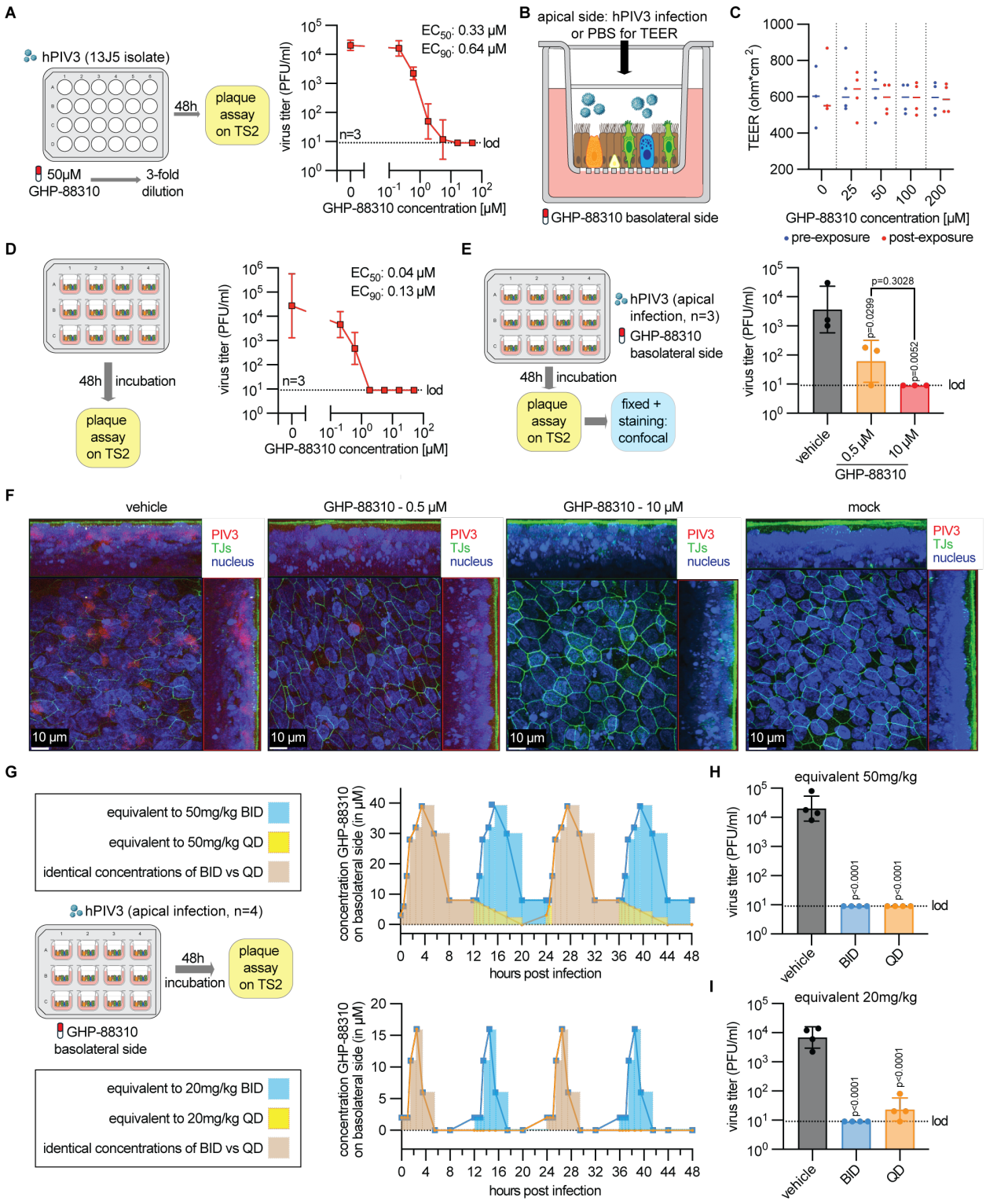

Figure 6. GHP-88310 efficacy in well-differentiated air liquid interface human airway epithelial cultures. A) Virus yield reduction of HPIV3 (clinical isolate 13J5) in undifferentiated NHBE cells (F3, n=3). **B)** Schematic of well-differentiated air-liquid interface human airway epithelial organoids. **C)** Assessment of GHP-88310 cytotoxicity in organoids. TEER was measured before and after 48 hours of

982 exposure to increasing concentrations of GHP-88310 in the basolateral chamber. Symbols represent
983 individual biological measurements, and lines show medians. **D)** Virus yield reduction assay of HPIV3
984 in organoids. Shed progeny virus was collected from the apical side of the transwells. Curves show 4-
985 parameter variable slope non-linear regression models, symbols represent the geometric mean ±
986 geometric SD. **E)** HPIV3 titers in infected organoids used for confocal imaging. **F)** Confocal microscopy
987 of organoids infected with HPIV3 at 2dpi. Cells were stained with anti-HPIV3 HN (red), anti-ZO-1 (tight
988 junctions; green), and Hoechst 34580 (nuclei; blue). Z-stacks of 100-150 0.22 μm slices with 63× oil
989 objective. Scale bar, 10 μm. **G)** *Ex vivo* PK-guided assessment of GHP-88310 efficacy against HPIV3
990 in organoids. The simulation recapitulates the PK profile of GHP-88310 following 14 doses of 50 mg/kg
991 b.i.d. (top) or the PK profile after 20 mg/kg q.d. Solid lines represent the experimentally measured PK
992 profiles in ferrets. Corresponding compound concentrations of GHP-88310 applied at each time point
993 are shown as bars. **H,I)** HPIV3 titers from the *ex vivo* simulation study. In (E,H,I), bars indicate the
994 geometric mean ± geometric SD and symbols represent individual biological repeats. One-way ANOVA
995 with Dunnet's (comparisons to vehicle) post-hoc multiple comparisons test. Group sizes (n) are
996 indicated in each study schematic.